UiT
THE ARCTIC
UNIVERSITY
OF NORWAY

Department of Geology

Seafloor craters and mounds in the central Barents Sea

—

Natalia Isaksen

EOM-3901 Master thesis in Energy, Climate and Environment June 2016

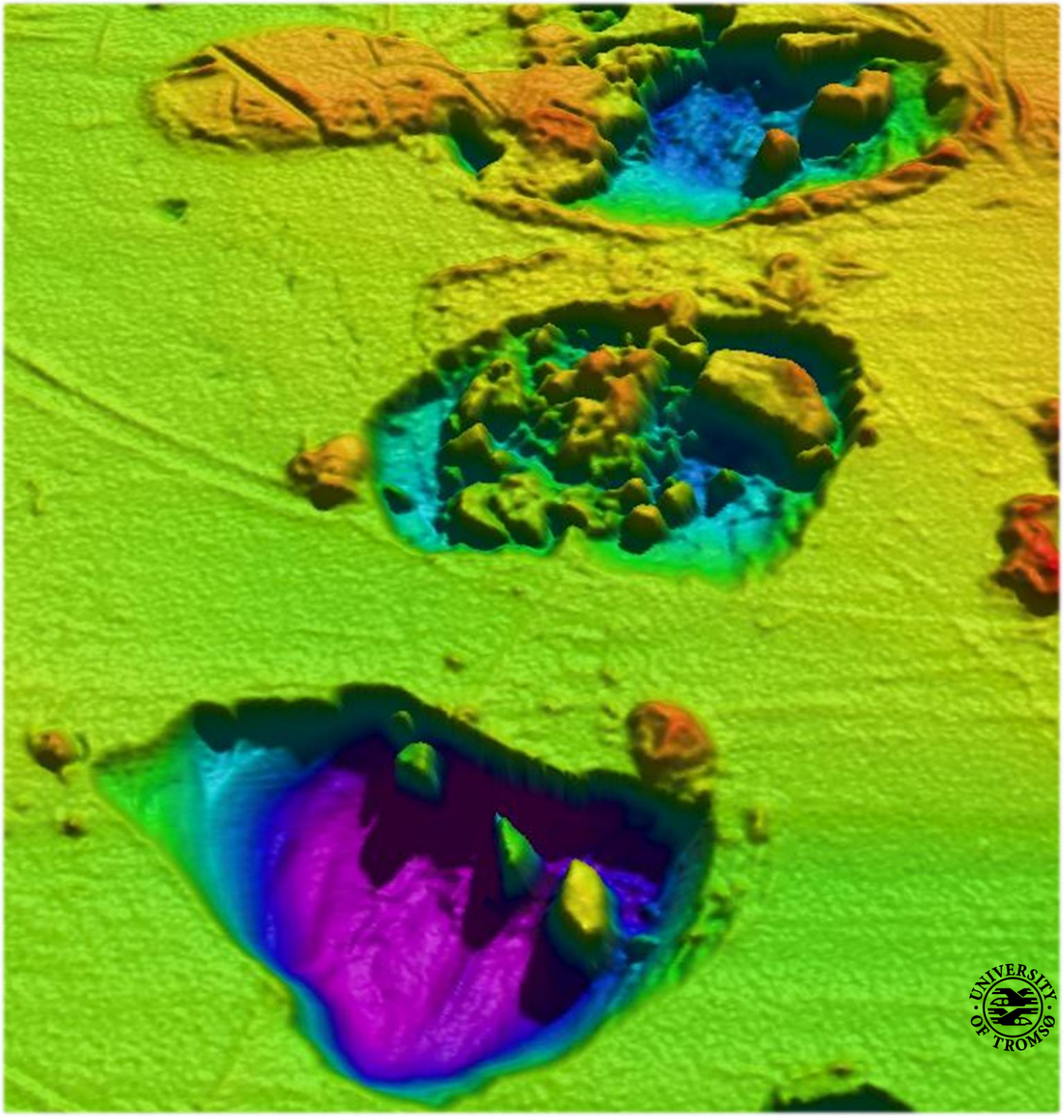

Abstract

Multiple giant craters and mounds have been identified in the area of the Upper Bjørnøyrenna in the central Barents Sea from the reflection seismic and echo sounder data. Analysis of seismic and echo sounder data revealed clear connection between these distinct seafloor features and seismic amplitude anomalies. Distribution pattern of the numerous water column anomalies registered in the area and interpreted to be gas plumes, corresponds to the location of faults in the study area what suggest that gas is of thermogenic origin and is migrating from the deeper reservoir through porous layers and faults working as vertical conduits. Suggested that craters and mounds are collapsed depressions and collapsed gas hydrate pingoes and their formation is associated with the processes of formation and decomposition of shallow gas hydrates due to the last glaciation period in the area, the Late Weichselian Maximum.

Acknowledgments

I would like to express my deepest gratitude to my supervisor, Professor Karin Andreassen, for her useful remarks, engagement and for all of the encouraging words, which kept me inspired during the work with master thesis. Furthermore, I would like to thank Monica Winsborrow, for her constant support and her meaningful and accurate comments. Also, I like to thank Sunil Vadakkepuliyambatta, Stefan Bünz, Kjersti Gausvik and all the lectors, researchers and advisers at The Arctic University of Norway in Tromsø for sharing their knowledge, answering questions and having their doors always open for me.
I am grateful to my dear friends and loved ones, who supported me through the entire process, for their care, patience and faith in me.

Without you, I would never be where I am now. Thank you all!

Table of Contents

1. Introduction

Gas hydrates have been widely reported along continental margins and polar regions where required conditions for their formation are probable to occur. In the shallow lithosphere, they form one of the largest reservoirs of methane in the global organic carbon cycle. (Kvenvolden et al., 2001) Seafloor seeps and associated features represent the venting points of methane released from the shallow subsurface to the water column and further to atmosphere. (Serié et al., 2012) Since 1970 when gas leakage-related features called "pockmarks" were first described by King et al. (1970) the increasing interest to investigation of areas with gas venting from the seabed is observed. Gas seepage itself as well as sedimentary features associated with gas or gas hydrates became the object of variable researches within the marine environment. Reasons for that are mainly seep's sensitivity to seismicity which makes them objects for geohazard monitoring, environmental impact of the methane from marine sediments, study of gas hydrates and also cold seep's significance for biology, as unique ecosystems are formed around them. (King et al., 1970; Etiope, 2015; Kvenvolden et al., 2001)

In the central Barents Sea, fields of semicircular, closed crater-like depressions have been reported and suggested to be formed due to gas release from the layers underlying the sea bottom. (Solheim et al., 1993; Lammers et al., 1995; Long et al., 1998) Number of water column anomalies registered in Upper Bjørnøyrenna suggests that active gas seepage occurs in the area. Multi-beam bathymetry data and echo sounder data from the part of the central Barents Sea were used to document in details multiple giant craters and prominent mounds, often in close proximity. Detailed seismic investigation supports suggestion that their origin is associated with the formation and decomposition of shallow gas hydrates.

All this observations makes the crater field in the Upper Bjørnøyrenna a prime interest to study seafloor deformation processes, active gas seepage within the area and role of gas hydrate in the dynamics of formation of craters and mounds.

2. Objectives

The principal objective of this paper is to acquire better understanding of the formation processes of distinct carters and mounds within the study area in the Upper Bjørnøyrenna, the central Barents Sea. Furthermore, it was considered relevant and important to map these prominent depressions and build-up structures, study their distribution pattern, internal structure and relation to the gas leakage from the seabed as well as to map seismic indications of fluid flow and faulting and observe the degree to which these correlate with the structures on the seafloor.

3. Settings

The Barents Sea

The Barents Sea is an epicontinental sea that covers one of the widest continental shelves in the world. It is bounded by Tertiary rift and shear margin to the north and west and by Novaya Zemlya to the east and by Norwegian and Russian coasts to the south. The Barents Sea is transected by several troughs, among them is the major Bear Island Trench (further in text: *Bjørnøyrenna (norw.)*) cutting the seafloor on east-west direction and two south-east to north-west trending troughs: Ingøydjupet and Djuprenna. Bathymetry of the Barents Sea is characterized by relatively flat seafloor, typically shallow banks of 100-200 m and average water depth of 250 m. Water depth within troughs increases up to 300-500m. (Andreassen et al., 2009; Solheim et al., 1993) Bathymetry map is shown on the Figure 1.

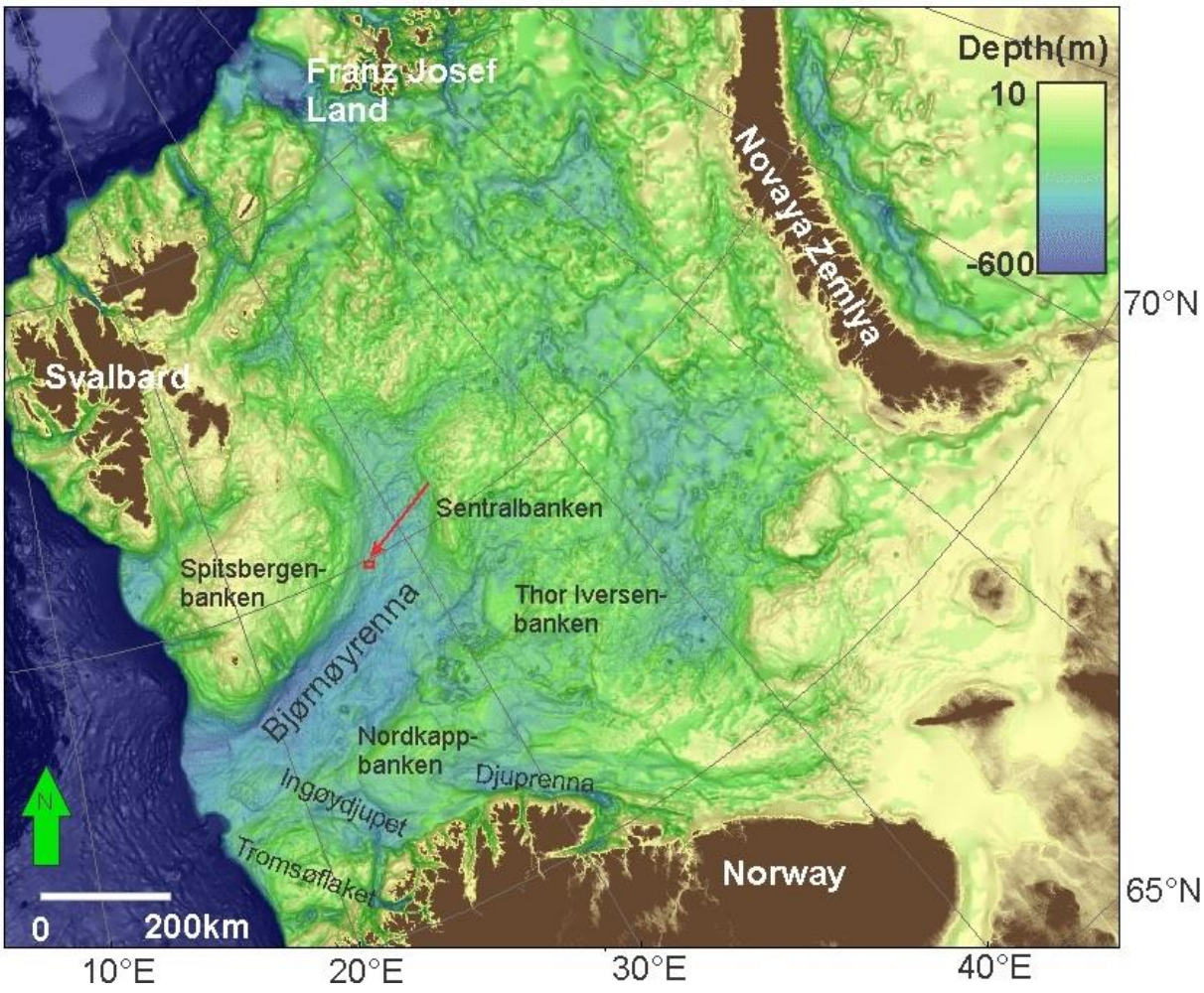

Figure 1. Bathymetric map of the Barents Sea with study area in Upper Bjørnøyrenna indicated by the red rectangle and arrow.

The Bjørnøyrenna

The largest and most prominent trough is Bjørnøyrenna. It extends 750 km from Sentralbanken to the shelf edge in the west. Width of the trough varies from 150 to 200 km different places. Bjørnøyrenna is bounded by shallow bank areas: Sentralbanken, Spitsbergenbanken to the east and north and Thor Iversen-banken, Nordkappbanken and Tromsøflaket to the south. This part of the Barents Sea is covered with a thin, less than 5 meters, layer of unlithified sediment with a relatively low organic content. (Solheim et al., 1993) Average water depth vary from less than 300 m to 500 m in the deepest central part. Bathymetry is demonstrated on the Figure 2a. The larger-scale seafloor geomorphology is characterized by several grounding zone wedges and sets of mega-scale glacial lineations (MSGL) extending to the shelf edge. Some of the MSGL in the western part of the trough are "larger than any of the onshore streamlined bedforms", with "lengths up to 180 km, widths up to 5 km and vertical relief up to 7 m". (Andreassen et al., 2008; Winsborrow et al., 2009) These landforms document the operation of an ice stream in the trough during the Late Weichselian glaciation.

The study area

The area surveyed covers about 36 km2 and is situated in the central Barents Sea at 74°54'N, 27°35'E in the upper part of Bjørnøyrenna. Its exact location and orientation is demonstrated on the Figure 2. Based on the data delivered by multi-beam echo sounder it was discovered that water depth in the area of interest vary mostly in range of 330 – 340 m but can be as deep as 360-370 m in a several depressions. The bathymetry within study area contains such distinctive features as deep crater-like depressions and rough, mostly uneven mounds. Apart from that, the morphology of the surrounding seafloor is rather smooth, although, additional features as smaller craters and the glacial related features, including mega-scale glacial lineations, iceberg plough marks and ice sheet retreat ridges, are observed.

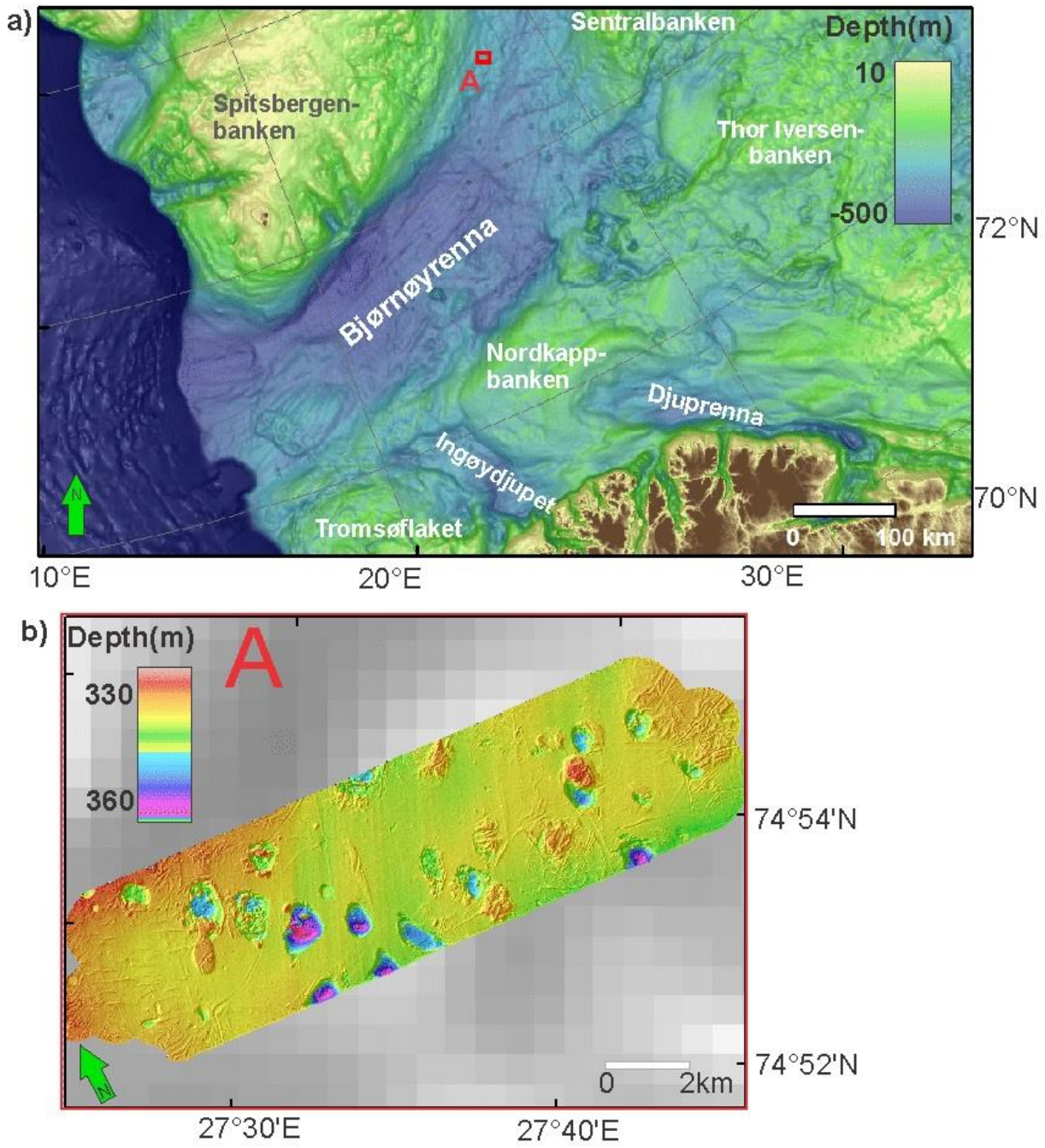

Figure 2. a) Map showing the bathymetry of the central Barents Sea. Study area is indicated by the red rectangle A; b) Closer view (1:30 000) to the red rectangle A demonstrating bathymetry and exact orientation of the study area.

4. Glaciation history: Late Weichselian Maximum

Major ice sheet was formed over the area during the Late Weichselian. Till overlain by glaciomarine sediments that date from Late Weichselian has been mapped on the seafloor of the most of Barents Sea and surrounding islands. One of the most convincing evidences of presence of grounded ice sheet was occurrence of subglacially-formed flute bedforms discovered in central Barents Sea in the Bjørnøyrenna and in the St. Anna Trough east to the Franz Josef Land. (Svendsen et al., 2003) Winsborrow et. al. (2009), based on the detailed bathymetry data and 3D seismic data, have proposed a five-stage reconstruction of the Late Weichselian deglaciation. Model is demonstrated on Figure 3.

Stage 1

At the Late Weichselian Maximum, ice covered the whole Barents Sea continental shelf. The footprint of the Bjørnøyrenna Ice Stream, extended to the shelf edge, was dominating in the glacial geomorphology of the Barents Sea shelf. According to Winsborrow et al. (2009), this ice stream had a length in approximately 600 km and a width of 165 km and was larger than the Hudson Strait Ice Stream and the Siple Coast Ice Streams of West Antarctica, reported to be of size of 800x90 km and 300x500 km, respectively. (Winsborrow et al., 2009; Vorren et al., 2011)

Stage 2

Deglaciation began with significant retreat of the ice sheet in the southern Barents Sea. The gradual retreat of an active ice stream is indicated by grounding zone wedges with MSGL on their surface in Bjørnøyrenna. The deglaciation occurred along the western Svalbard margin and in Storfjordrenna. This early deglaciation stage is assigned an age of approximately 17 cal ka BP, based on radiocarbon dates form Tromsøflaket and Andfjørden. In the east, ice sheet configuration yet remained at the stage 1 and the ice extent had not reached its maximum. (Vorren et al., 2011; Winsborrow et al., 2009)

Stage 3

The next stage is characterized by significant change in the dynamics of ice sheet with eastward shift of the center of maximum ice volume and the deglaciation of the large part of the southwestern Barents Sea. Tromsøflaket and the deepest part of Bjørnøyrenna were ice-free, but the area of interest for this paper located in the upper part of Bjørnøyrenna was still covered

with ice. The ice margin has retreated closer to the coastal line along the western continental shelf. Djuprenna and Nordkappbaken-east Ice streams were major readvanced, but Bjørnøyrenna Ice Stream was still active and has its position marked by the grounding-zone wedge situated 250 km from the shelf break, according to Winsborrow et. al. (2009). Stage 3 is suggested to represent approx. 16 cal ka BP indicated by glaciomarine conditions in mid-Ingøydjuppet by 15,7 cal ka BP. (Winsborrow et al., 2009; Vorren et al., 2011)

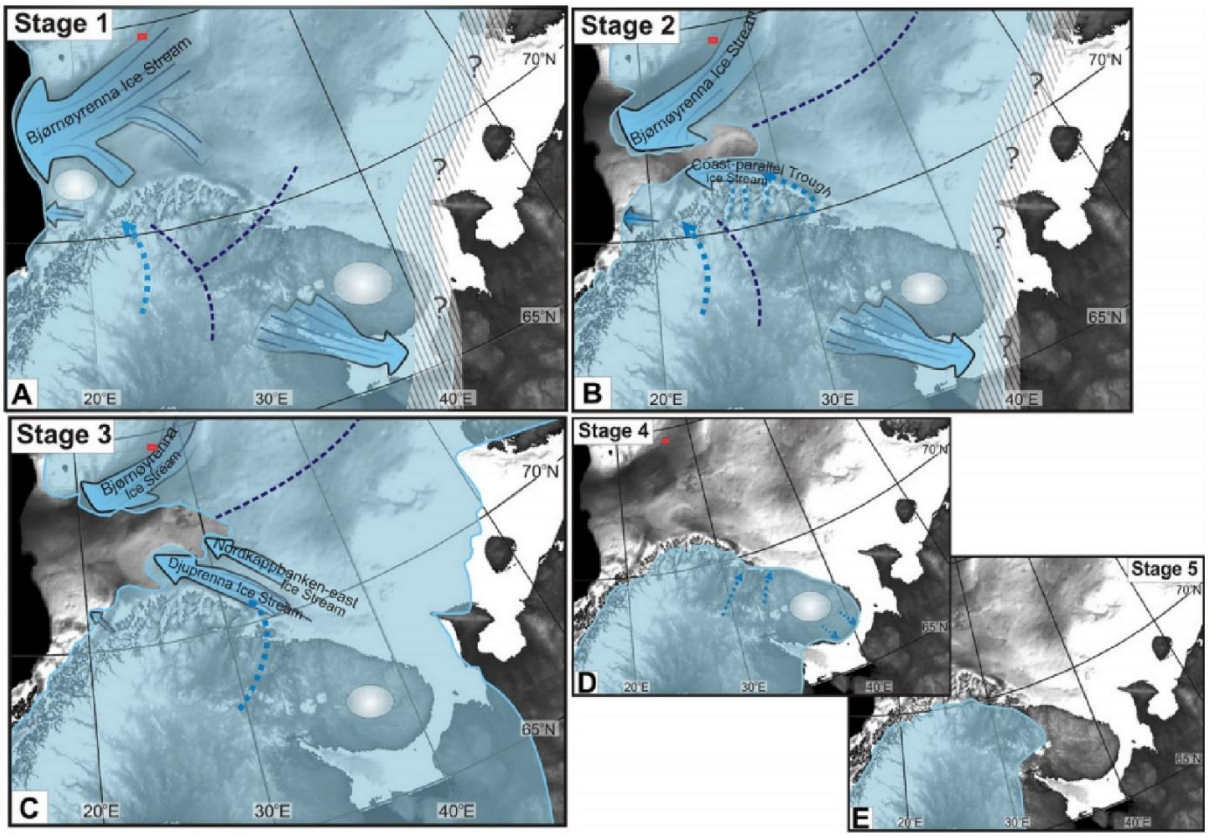

Figure 3. Five-stage reconstruction of the Late Weichselian maximum and deglaciation of the southern Barents Sea. Ice streams are shown as large blue arrows, warm-based ice as dashed blue arrows, cold-based ice as white discs and possible ice divides as dashed dark blue lines. Red rectangle marked on the stages 1- 4 shows location of the study area. Modified from Winsborrow et al. (2009), fig.10.

Stage 4 and 5

By stage 4, assigned an approximate age of 15 cal ka BP, the southern and central Barents Sea are completely ice-free while ice margin is located in the outer-fjord area in northern Norway and Kola Peninsula. Stage 5 marks the significant retreat of the ice cover to the west of Kola Peninsula and southwards in northern Norway. (Winsborrow et al., 2009)

5. Seismic indications of fluid migration

Gas generated beneath the seafloor is buoyant and tends to migrate towards the surface. (Judd et al., 2007) There exist various different approaches, which can be used to identify evidence of shallow gas presence and fluid migration from geophysics datasets, and following section details some of those methods.

Columnar disturbances and seismic chimneys

Focused fluid flow vents from the underlying source region and forms vertical to sub-vertical pathways, which are recognizable on the seismic profile as columnar zones of disrupted reflection continuity extending across layered succession. Terminology associated with focused fluid flow related structures are potentially confusing as they may be referred to as fluid escape pipes, gas pipes, acoustic pipe structures, blow-out pipes, gas chimneys or seismic chimneys. The wide range of terms partly reflects continuity of the processes involved in structures formation, scale and seismic expression. Acoustic pipes are sub-vertical, narrow zones of acoustic masking with reflection continuity disrupted over some vertical extent. Identifying of the root zone of a pipe could be helpful and important to make connections with source region of fluid involved in pipe genesis. An upward limit of the seismically visible pipe structure is called pipe terminus and may provide important information related to pipe genesis, growth and timing. (Cartwright et al., 2015; Andreassen et al., 2007)

High amplitude anomalies

Amplitude anomaly is an abrupt change in seismic amplitude, indicating sudden changes in acoustic impedance, product of the compressional wave velocity and density. (Andreassen et al., 2007; Gillis, 2016) Presence of the free gas in the subsurface causes a significant reduction of compressional wave velocity, and will give rise to a reflection with anomalously high amplitude. One of the principle features are bright spots that are marked by high amplitude reflection from the top of the gas, which have negative reflection phase while seafloor reflection represent positive phase. They express increase in gas content within sedimentary horizon. Although, gas is not the only cause of such a feature as bright spot which is a result of impedance contrast between adjacent media. (Hovland et al., 1988; Judd et al., 1992)

Acoustic masking

Acoustic masking or acoustic blanking in sediments represents an area where seismic reflections are highly distorted and disturbed due to very poor reflection and scattering of the seismic wave. This is an amplitude anomaly typical for gas-affected zones and may result from the disruption of sediment layering by the migration of pore fluid or be caused by the absorption of acoustic energy in overlying gas-charged sediments. Relatively low amplitude return signal can be also caused be the reflection of a large proportion of acoustic energy by an overlying hard sediment. (Jamaludin et al., 2015; Hovland et al., 1988; Andreassen et al., 2007)

Velocity anomalies

Such velocity anomaly as pull-down effect – "smile"- occur often at the edge of acoustic blanking. There is an indicator of the decrease in the seismic velocity and is caused by increase in gas content, but not to the point at which acoustic blanking will occur. (Hovland et al., 1988)

6. Gas hydrate

Gas hydrates are crystalline, ice-like solids composed of rigid cages of water molecules that enclose guest gas molecules, usually methane. They are widespread on the 90% of continental shelf. Gas hydrates are formed in the pores of seabed sediments under conditions of low temperature, high pressure and certain gas concentration (at least 5-10% of gaseous methane should be presented for formation of methane hydrate). They are stable at certain pressure-temperature equilibrium, but a modest increase in temperature or decrease in pressure may lead to decomposition. In this case, gas will be released with the potential for migration to the surface, water column and further to atmosphere. (Etiope, 2015, Long et al., 1998, Paull et al., 2007) Gas hydrate pingoes are generally formed due to growth of hydrate in the shallow subsurface. Their formation requires continuous high flux of gas-saturated pore fluid to maintain high methane concentration within the sediments to prevent dissociation of hydrates and usually suggests supply of hydrocarbons of thermogenic origin. Gas hydrate pingoes have been observed in multiple places around the world: Beaufort Sea, Northern Gulf of Mexico, Barkley Canyon in Canada, offshore California, Japan. (Serié et al., 2012; Paull et al., 2007; Etiope, 2015)

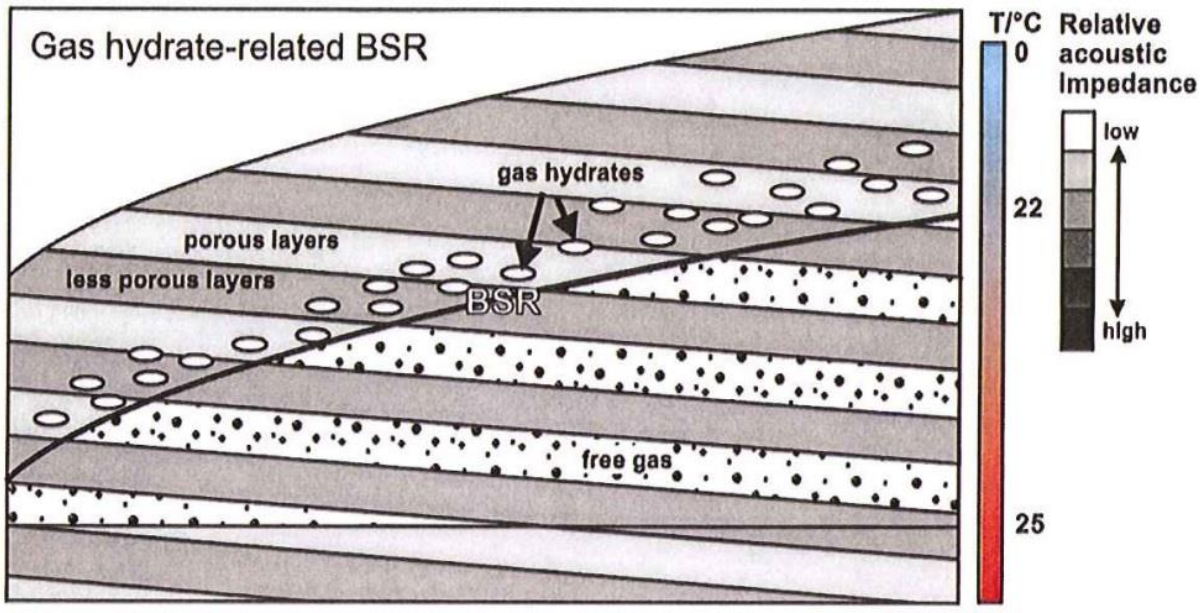

Figure 4. Sketch representing changes in acoustic impedance and their causes. Schematic temperature bar indicates typical temperatures for the processes. Modified from Berndt et al. (2004), fig.5.

Gas hydrate stability zone refers to a zone at which gas hydrates naturally exist in the subsurface. Although, it is primarily dependent on temperature and pressure conditions, other

factors as gas composition may influence stability boundaries. The existence and depth of gas hydrate stability zone is often seismically indicated by bottom simulating reflector (BSR) that indicates the lower limit of the gas hydrate stability in sediments. Gas hydrate-related BSR is roughly parallel to the seafloor reflector and is caused by a density contrast between overlying gas hydrates and gas-saturated sediments underneath. (Cartwright et al., 2015; Berndt et al., 2004; Sheriff, 2002)

7. Data and methods

Most of the data used in this paper were collected during the marine geological cruises on *R/V Helmer Hansen* in July 2015 but partly also in 2014 and 2013. Study is based mostly on the high-resolution multi-beam and single-beam echo sounder data from the area of interest and 3D reflection seismic data. 2D seismic were used to get better regional understanding of the area.

High resolution 2D seismic

For this study, 2D reflection seismic acquisition were provided using two mini GI (Generator-Injector) air guns with total volume of 60 in^3, which are especially suitable to get high-resolution data. Shooting rate was 3 seconds and the sampling rate - 0,25 ms. Data have been processed on-board in Radex-Pro for quality control and then imported to Petrel for further independent analysis. (Center for Gas Hydrate, Environment and Climate (CAGE), 2015) Additionally, several 2D seismic lines used in this study were provided by Norwegian Petroleum Directorate (NPD). Location of the seismic 2D lines is demonstrated on Figure 5.

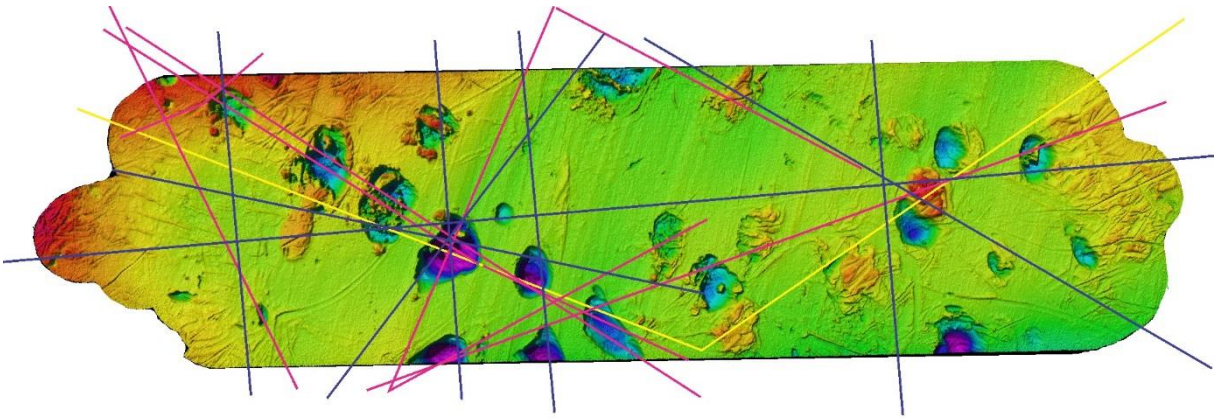

Figure 5. Bathymetry map of the area surveyed showing location of the seismic 2D lines: Rose and yellow lines were collected by CAGE during marine geological cruises in 2014 and July 2015, respectively; blue lines were provided by NPD.

High resolution 3D seismic

Although, both 2D and 3D seismic are based on the principle of penetration of the surface by sound waves to record lithological changes in the subsurface and were used to study deeper subsurface, 3D seismic allows imaging of deeper structure and stratigraphy with relation to the seafloor features and to analyze continuity of features of subsurface. During 3D reflection seismic survey, the P-Cable 3D high-resolution seismic system including 14 streamers 25 m

long each, were used. It allowed to cover large area with close channel spacing at 3,125 m. Shooting rate during 3D seismic survey was 6 seconds and sampling rate – 0,50 ms. After on-board data processing in Radex-Pro for quality control and in Petrel, data were imported to Petrel for further analysis, which were provided independently for this study. Frequency of the 3D seismic vary in range 20Hz - 250Hz after processing, but average frequency is about 100-150 Hz as shown on Figure 6. (Center for Gas Hydrate, Environment and Climate (CAGE), 2015)

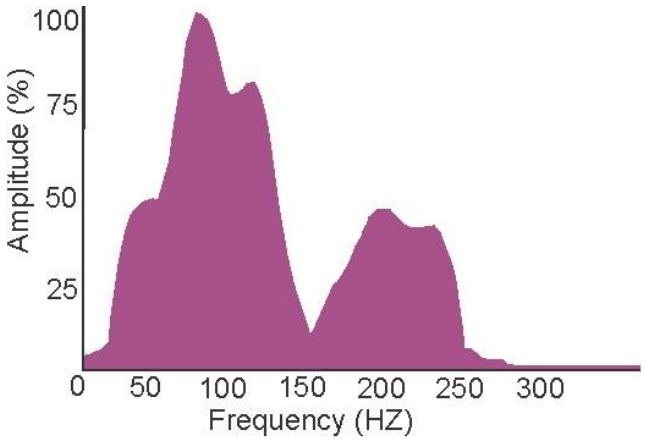

Figure 6. Frequency (Hz) vs Amplitude (%) graph compiled based on the migrated 3D seismic data used in the current investigation.

Echo sounder data

High resolution bathymetry data were collected using hull-mounted Kongsberg Simrad EM 300 multi-beam echo sounder with wave frequency 30 kHz. The outer beams of the EM 300 can be of low quality due to speed and reception of signal errors so to prevent loss in quality there is usual overlap between tracklines about 7-25%. Programs Fledermaus and ArcGis were used to visualize and process the data. The backscatter data were acquired abroad *R/V Helmer Hansen* using a keel-mounted Simrad EK 60 single beam echo sounder. Transducer at frequency 18 kHz were used to detect gas leakage from the seafloor. Distance between the tracklines is 60 m. (Center for Gas Hydrate, Environment and Climate (CAGE), 2015) The water-column backscatter data were evaluated to identify anomalies using the software Fledermaus Midwater. Gas flares were mapped on the bathymetry of study area using Fledermaus and FM Midwater. Independent visual analysis was made to qualify gas plumes and a subjective quality factor from 1 to 9 was assigned to each flare.

8. Results

8.1 Seafloor geomorphology

A range of the geomorphologic features on the seafloor within the study area provides information about two main processes: deglaciation and release of the free gas from subsurface.

8.1.1 Glacial geomorphology

Straight linear ridges

Description

Large elongated ridges are observed in the central part of the area surveyed. They are up to 2,3 km long and 0,35-0,8 m wide The individual lineations have relief of up to 1,5 m, but averagely it varies in range 0,5 – 1 m. Elongation ratio of the lineations is up to 33:1. These features are barely recognizable on the seismic sections, but can be well seen on the shaded relief map (blue lines on the Figure 7b).

Interpretation

The streamline lineations observed on the study area of Upper Bjørnøyrenna are interpreted to be mega-scale glacial lineations (MSGL) produced by a fast-flowing grounded glacier. This interpretation has been made on the base of previous studies reporting similar features from the marine environments in Antarctica, offshore of Norway and Canada, where they appear in the areas occupied by fast-flowing ice streams. (Andreassen et al., 2008)

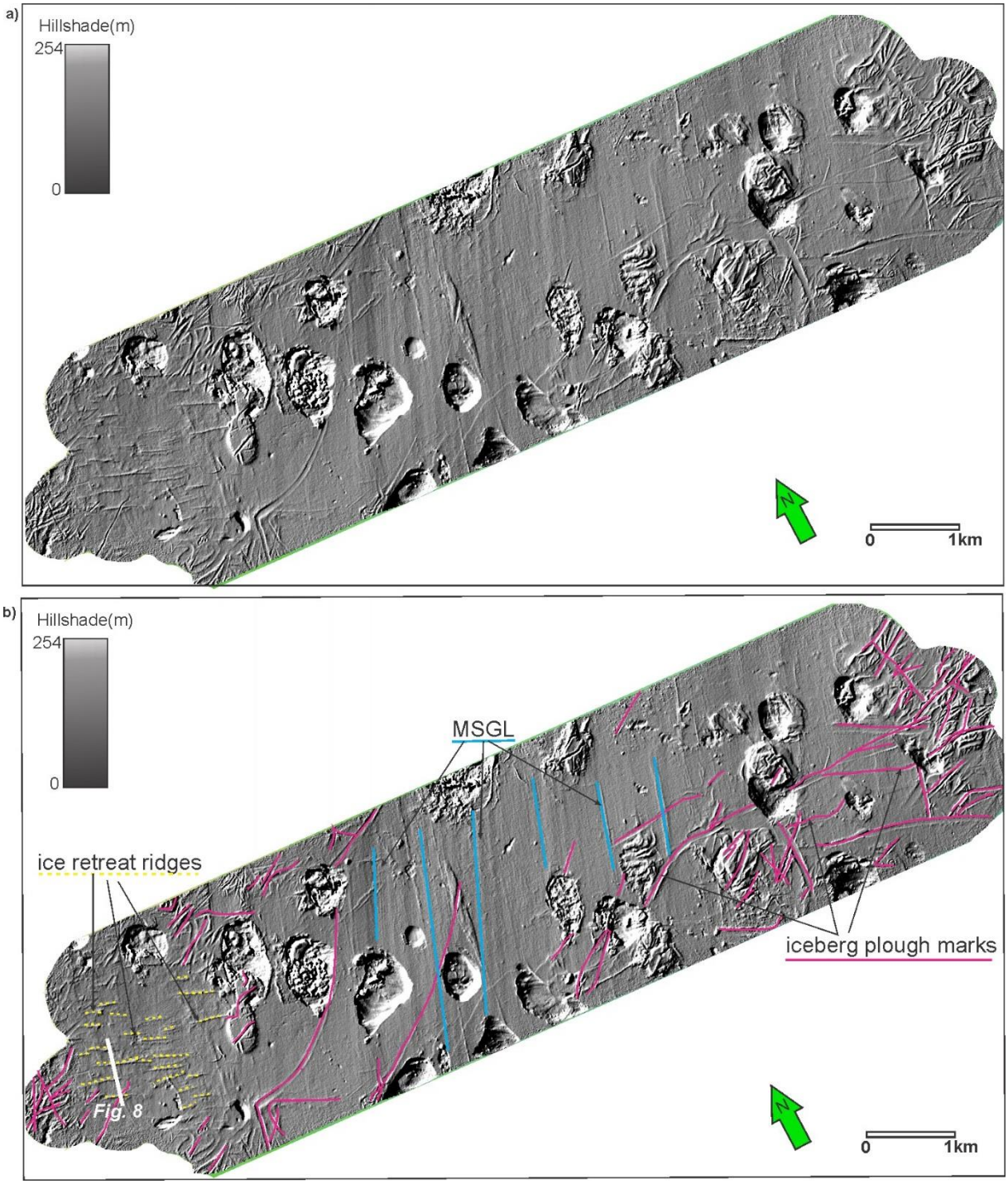

Figure 7. a) Shaded map of the study area in Upper Bjørnøyrenna; b) The same image as (a), with main glacial geomorphological features indicated: dashed yellow lines - ice sheet retreat ridges; solid blue and rose lines - mega-scale glacial lineations (MSGL), and iceberg plough marks, respectively. Location of bathymetry profile shown on Figure 8 is marked by solid white line.

Linear curved furrows

Description

Prolonged linear furrows occur at all parts of study area. Their distribution is shown on the Figure 7b where they are marked by solid rose lines. Features are often curved and U-shaped in cross-profile and vary significantly in length, depth and width both between furrows and within a single furrow. Orientation is random to preferred in west-east direction. Features are typically 2 m to 70 m wide and may be followed for up to 4 km. Common for these furrows is to have levees at their sides from few cm to 1 m high. Maximal relief is 1 m and structures are clearly visible on the shaded bathymetry map but are barely recognizable on the seismic profile.

Interpretation

Linear curved furrows on the seafloor are morphologically similar with features, which has been reported from other areas of the central and southwestern Barents Sea as Ingøydjupet, Djuprenna and Tromsøflaket, and are interpreted to be iceberg plough marks. (Andreassen et al., 2008) There are erosional structures caused by movement of icebergs by currents and wind along the seabed before final smelting of the glacier. Scouring of the seafloor is a very common feature in front of marine glacier and can lead to overprinting of previously formed geomorphological features but, in case of the study area, iceberg plough marks only erode and do not erase the underlying structures. (Andreassen et al., 2008; Benetti et al., 2010)

Parallel elongated ridges

Description

Mainly only on the western slightly uplifted part of the study area where water depth vary between 337 and 333 m, small elongated ridge structures are recognized (Figure 8). Preferred orientation is west-east and they are typically occur parallel to each other. About 30 of these ridges are concentrated on the area of 3 km^2 and are not presented or completely eroded on other parts of area of interest. Their location is presented on the figure 5. Ridges are 15-50 m wide with length varying in range 100-700 m. Relief is from 40 cm up to a slightly over 1 m.

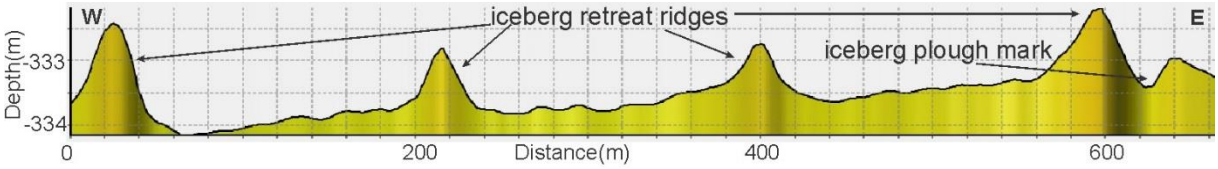

Figure 8. Bathymetry profile demonstrated iceberg retreat ridges and iceberg plough mark within the study area. Location is marked on Figure 7b.

Interpretation

Based on morphological and morphometrical properties of the elongated ridges discovered on the study area two main preposition according to interpretation were made: glacial flutes and ice sheet retreat ridges. However, orientation of the described features perpendicular to the ice stream makes the first preposition extremely improbable. Therefore, small parallel ridges have been interpreted as ice sheet retreat ridges. Possibly, they were formed by meltwater flowing under the glacier and depositing sand and gravel in form of elongated tails, which were left standing after the glacier retreated. (Lucas, 2015)

8.1.2 Craters and mounds

Description

In the study area, there are 18 large crater-like depressions of different shapes and diameters (Figure 9). Most of them have relief of 20-25 m and up to 35 meters, few are about 2-5 m deep but are still easy to identify on both the bathymetry map and seismic profile. Depressions have circular slightly prolonged to elongated shape stretching in two main directions: northeast - southwest and northwest –southeast. The individual craters can be up to over 900 meters long and 150 to 650 meters wide. Their elongation ratio are up to 2.5:1. Some of the depressions contain internal steep-sided mounds and ridges, rising as high as, or even greater than the crater walls. Numerous smaller scale depressions are spread around the whole study area but are slightly tighter distributed in the western and central parts than at the east. They have average diameter of 30-40 m, but individual depression can be up to 90m wide. These structures has oval to circular shape and relief varying in range 0.5-2m. Mound structures are represented by large formations in different shapes up to 17 m high, located just within the craters rim and nearby on the seafloor. There are characterized by lack of internal structures. It is typical for mounds in the study area to be eroded on top by what has be interpreted as iceberg plough marks. Depression and mound are often described together as a single feature because of close proximity.

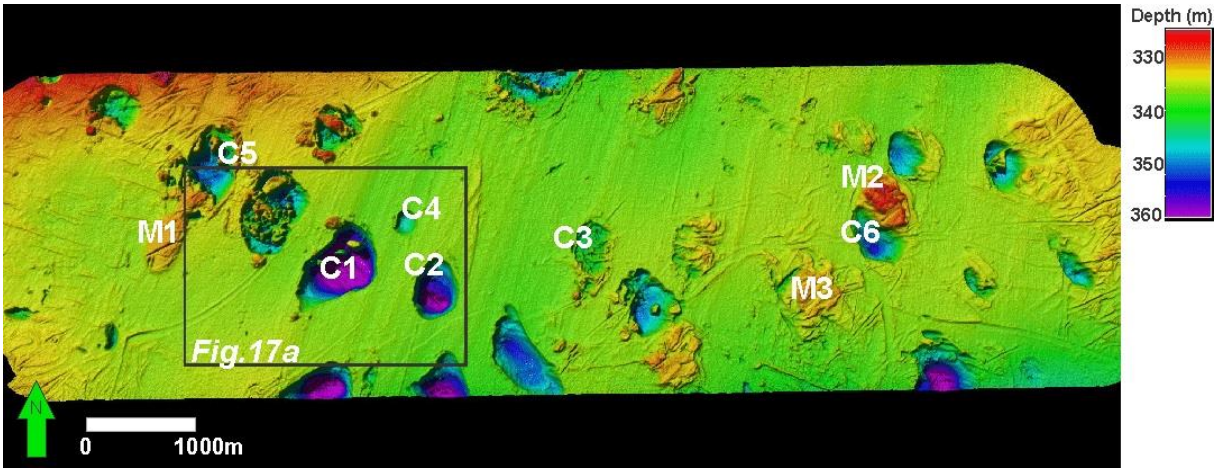

Figure 9. Bathymetry map of the study area in Upper Bjørnøyrenna. Location of craters and mounds, named C1-C6 and M1-M3, respectively, which will be discussed further in this paper, is demonstrated.

There is no direct correlation between location and size of the structures, although, based on the existing multi-beam echo sounder bathymetry map, the deepest depressions occur closer to the central part of the study area with highest water depth while the most pronounced build-up structures are absent in the center and concentrated in the both western and eastern slightly uplifted parts. Next several paragraphs are devoted to detailed description of several representative craters and mounds (Figures 10- Figure 17), named C1-C6 and M1-M3, whose location is demonstrated on the Figure 12, as well as smaller-scale structures marked on the Figure 17.

Crater C1

Structure C1 shown on Figure 10b has a shape of an irregular oval prolonged in northeast-southwest direction with maximal length of 980 m, and width varying from 250 m in the northern end to 550 m in the middle part and to approximately 90 m in the southwest. Depression is 29 m deep and has extremely steep slope of 69° at the western side opposite to more gentle one of 14° at the East, as shown on Figure 10d and Figure 10e. There are two mounds rising from the craters floor almost to the level of the crater rim and one more a few meters higher (Figure 10d). A fourth mound is much smaller and is located on the western sidewall of the crater. Internal mounds are demonstrated closer on the Figure 10c.

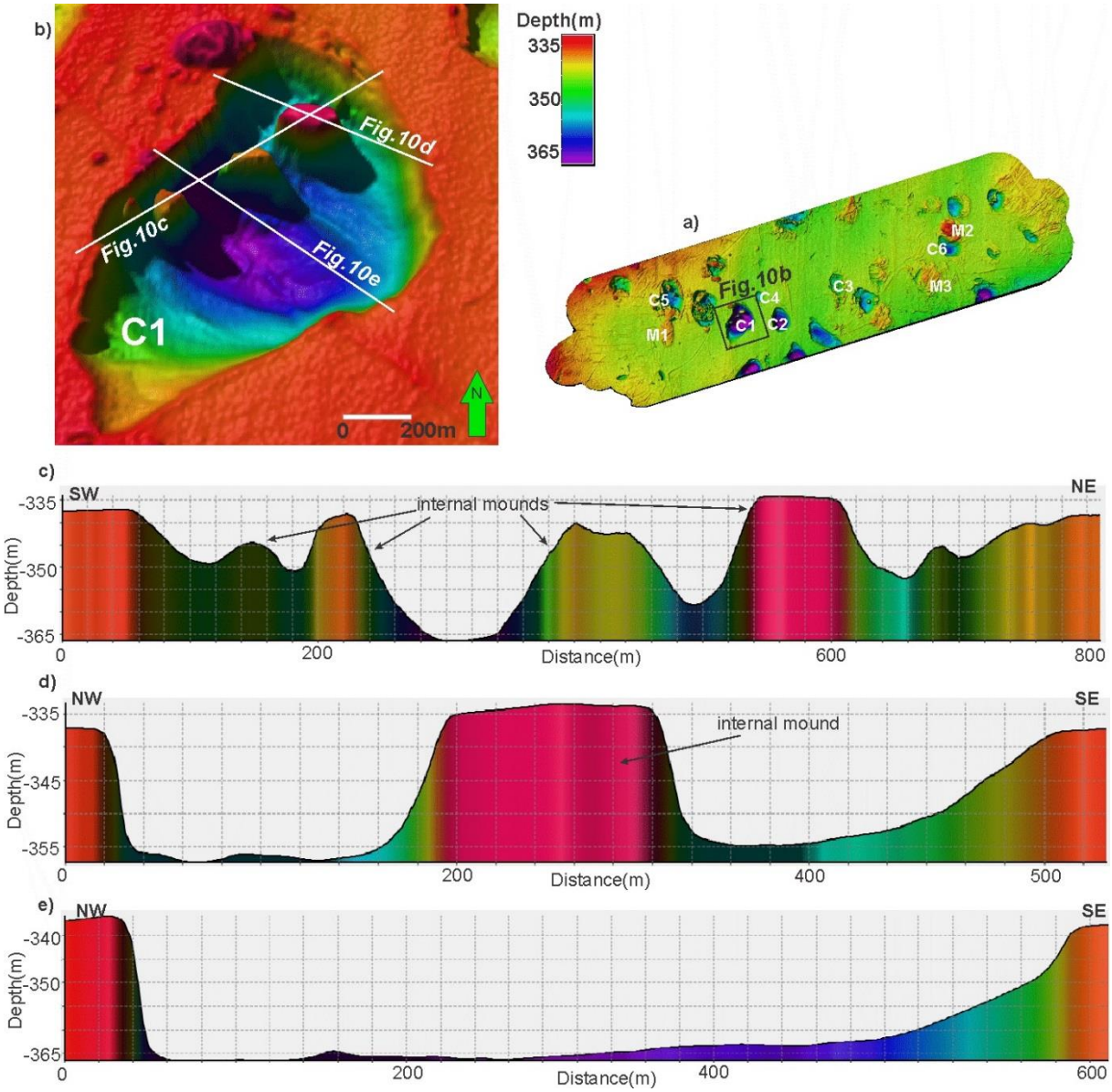

Figure 10. a) Bathymetry map indicating location of (b); b) Perspective image of crater C1; c, d and e) bathymetry profiles across crater C1 with location indicated in (b).

Crater C2

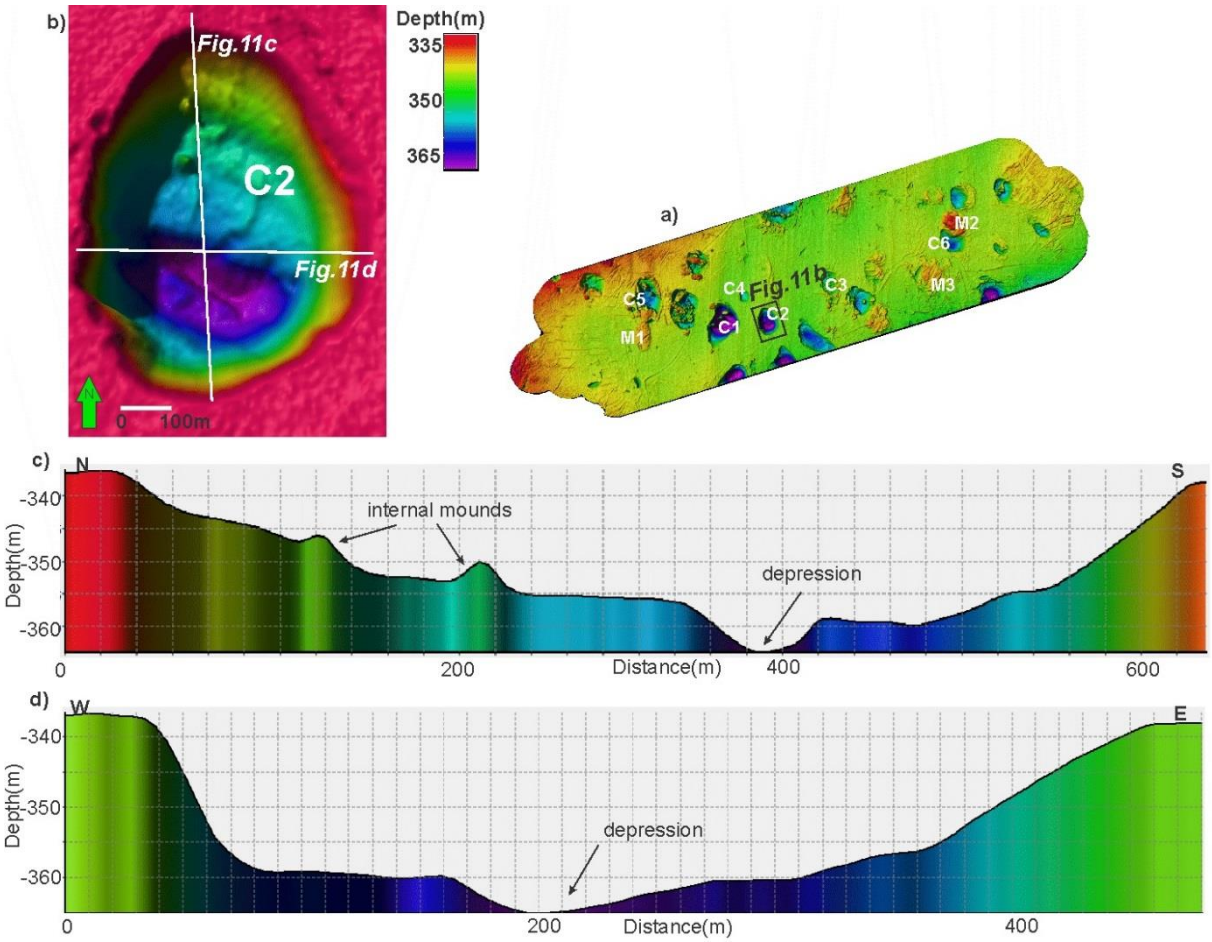

Figure 11. a) Bathymetry map indicating location of (b); b) Perspective image of crater C2; c and d) bathymetry profiles across crater C2 with location indicated in (b).

Crater C2 has north-south orientation and is located in the central part of the study area less than 500 m from the structure C1, as shown on Figure 11a. It is shaped as an oval and has maximal width of 430m and length of 590 m (Figure 11b). Average depth is 18 m but steep depression on the crater floor causes the maximal depth of the structure to be 25 m (Figure 11d). Two internal mounds 3 and 2.5 meters high are located in the northern part of the crater and can be seen on Figure 8c.

Crater C3

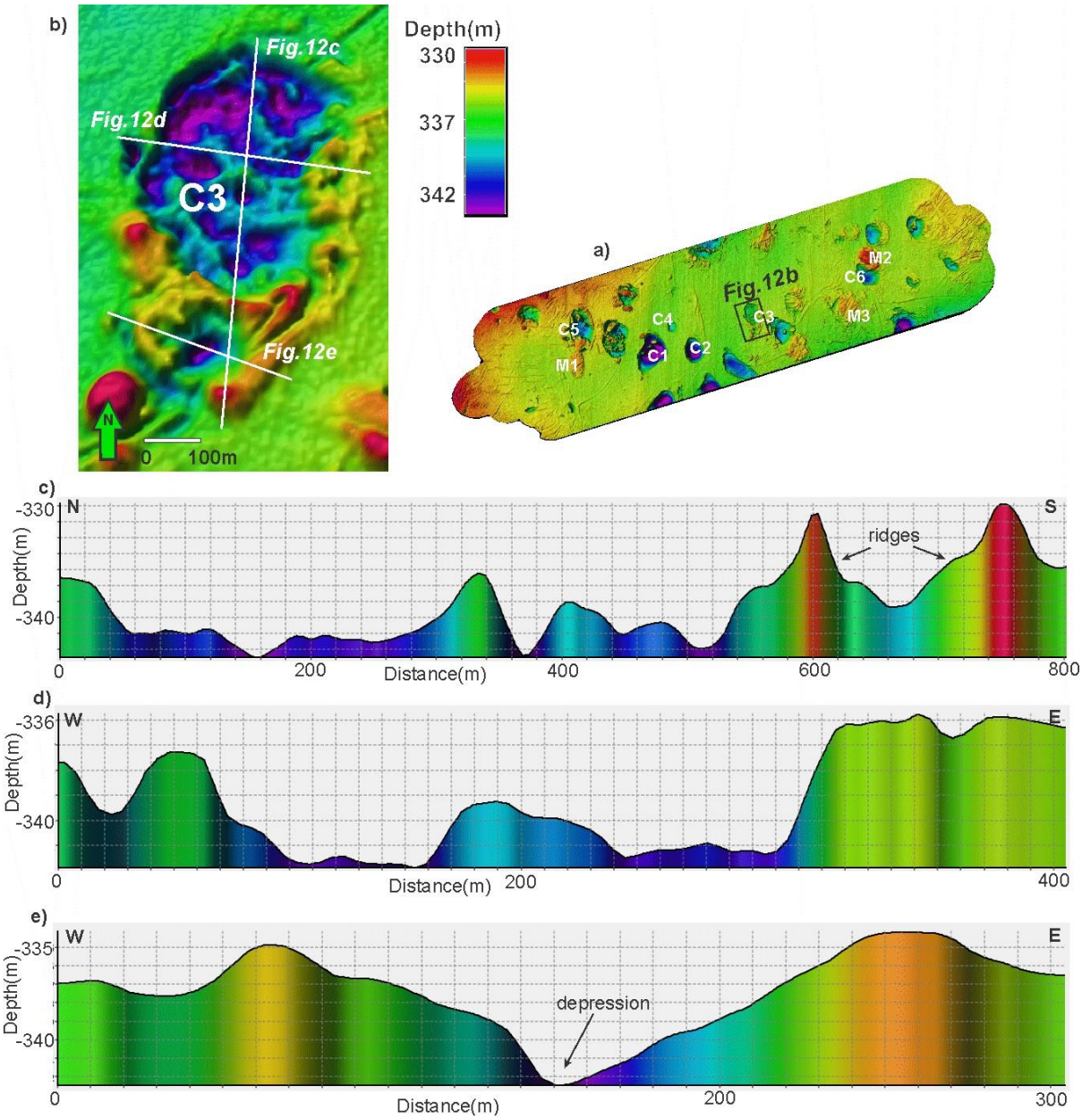

Figure 12. a) Bathymetry map indicating location of (b); b) Perspective image of crater C3; c, d and e) bathymetry profiles across crater C3 with location indicated in (b).

Structure C3 is located 1.2 km in the central part of study area, east from the depression C2 and is orientated in north-south direction (Figure 12a). There is complex structure consisting of multiple connected sets of depressions and ridges on the seafloor and is shown closer on the Figure 12b. Maximal depth of the depressions is approximately 7 meters. Length and width of the depression is 660m and 450 m, respectively. Randomly orientated mounds and ridges cover crater floor forming pattern of several sets of small depressions and build-ups (Figure 12c,d).

Ridge on the rim of the crater consists of several mounds 1-3 m high and divides crater from another structure. Part of the seafloor with diameter of 160 m at the southern edge of the C3, is surrounded by three ridges with average height of 2 m and individual peaks rising up to 3.5 m. Profile across it is demonstrated on the Figure 12e. 7 meters-deep depression in the middle is formed by mounds sidewalls with slopes of 4° at the east and 12°-17° on the other sides.

Crater C4

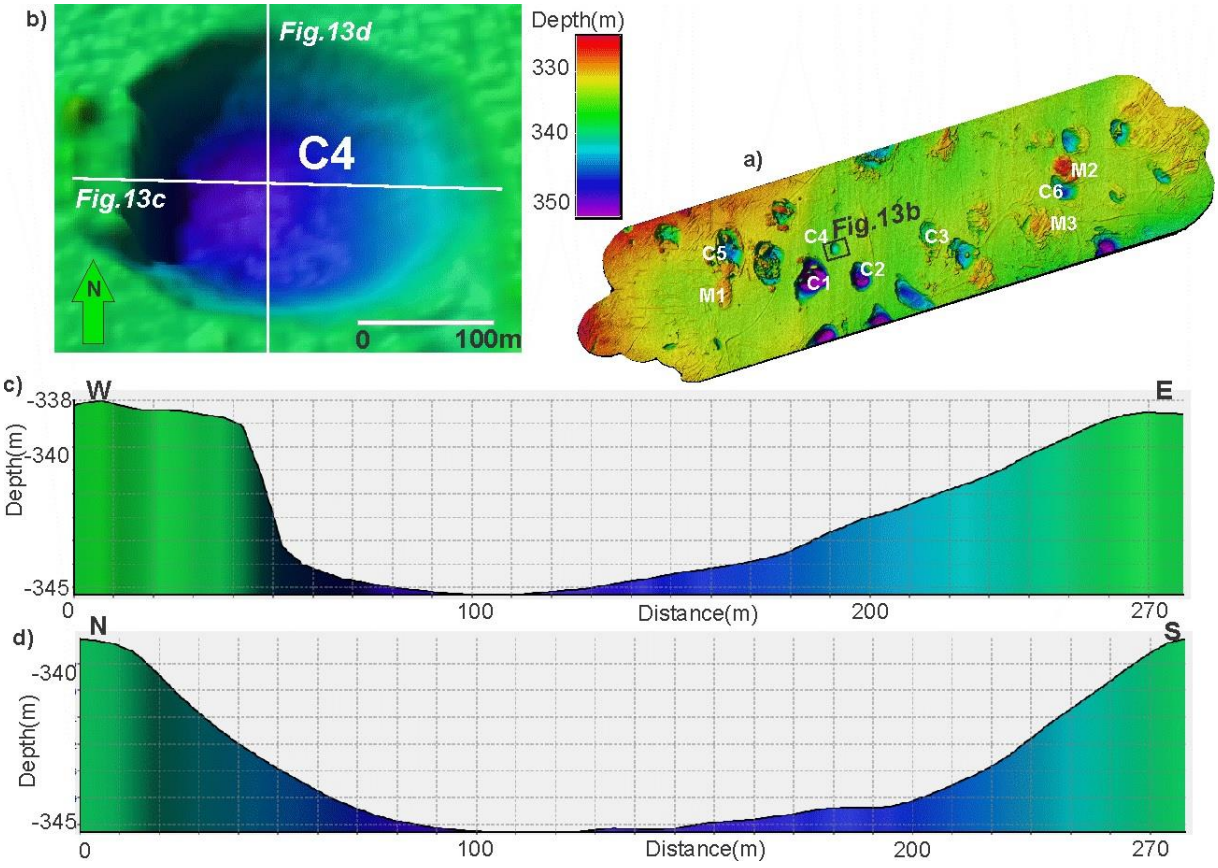

Figure 13. a) Bathymetry map indicating location of (b); b) Perspective image of crater C4; c and d) bathymetry profiles across crater C4 with location indicated in (b).

Structure C4 is situated close to the crater C1 in north-east direction. Depression has nearly ideal circular shape and diameter of 270 m. Relief is 6-7 m as shown on Figure 13. The western side of the crater B has a very steep slope of 26° while slopes from other sides are much more gentle and averagely equal to 4-6°. There are no internal structures on the crater floor or at the rim.

Crater C5 and mound M1

Complex structure, shown on Figure 14, northeast to the crater C1 has northeast-southwest orientation and is easily divided on two structures: depression and mound, C5 and M1, respectively. Crater C5 is about 700 m long and 500 m wide with maximal depth of 24 m. Similar to the most of the depressions nearby it has very steep western slope of 34° and gentle eastern one. Two stand-alone internal mounds is located on the crater floor and the third one - on the western sidewall. All of them are approximately 20 m high and rise up to the craters rim. There are also multiple build-ups with height of 5-8 m at the edge of the crater, surrounding it.

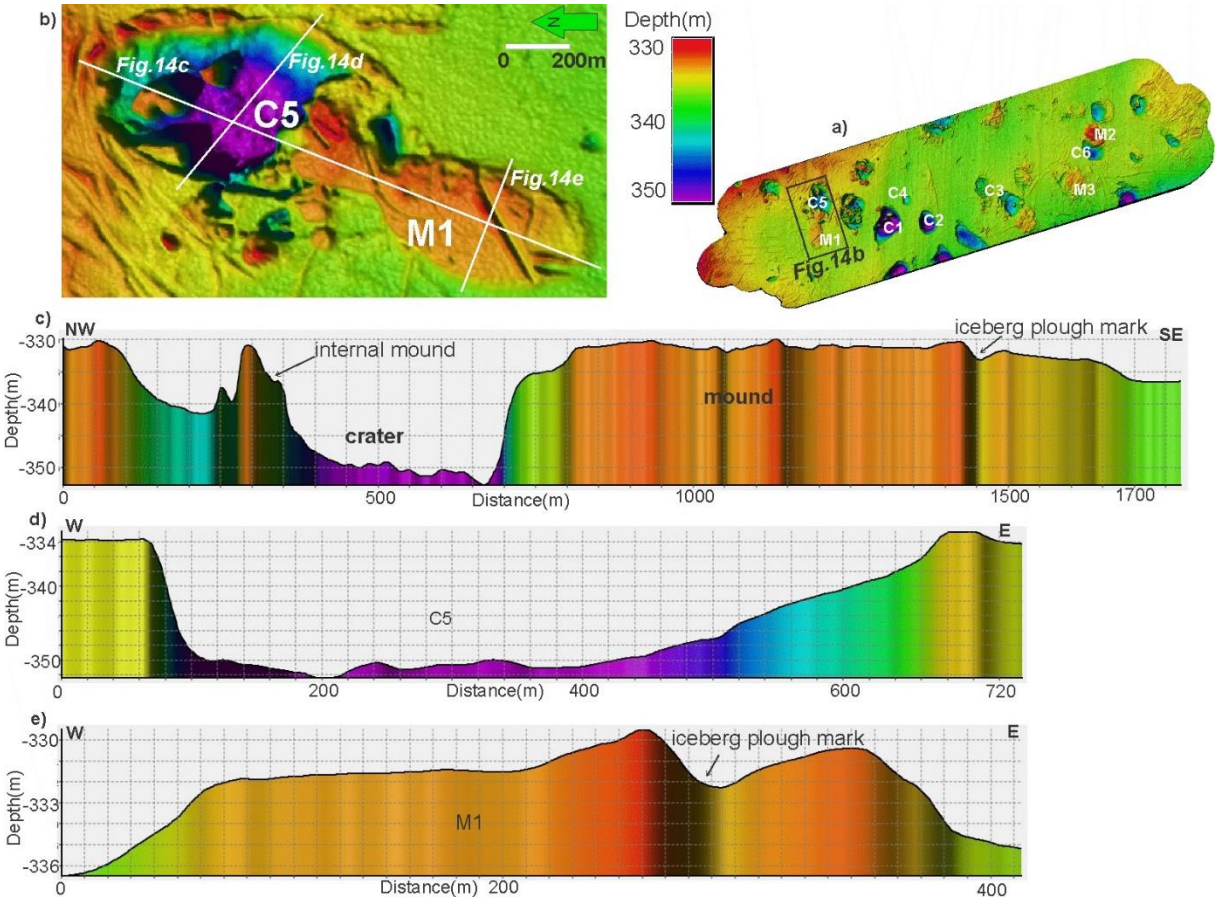

Figure 14. a) Bathymetry map indicating location of (b); b) Perspective image of crater C5 and mound M1; c) bathymetry profile across the whole structure C5-M1 with location indicated in (b); d and e) bathymetry profiles, with location indicated in (b), across the crater C5 and mound M1, respectively.

Structure M1 is the elongated oval-shaped mound with maximal relief of 6 m. Mound is 900 m long and 330 m wide, has quite smooth surface and no recognizable peaks of single mounds it could has been composed of, based on the cross-section profile. Structure is eroded on top by

several iceberg plough marks. The most pronounced one is 2 m deep with rather large levees on sides, and crosses mound in northeast-southwest direction.

Crater C6 and mound M2

Structure composed of crater, named C6, and mound – M2 is located at the eastern part of study area and is orientated in northwest-southeast direction. Their location and structure is closer demonstrated on Figure 15. Crater has length of 650m and width varying in range 270- 370 m. Several insignificant internal mounds on the crater floor and at the sidewalls with height less than 50 cm are presented. Maximal relief of the depression is equal to 20 m.

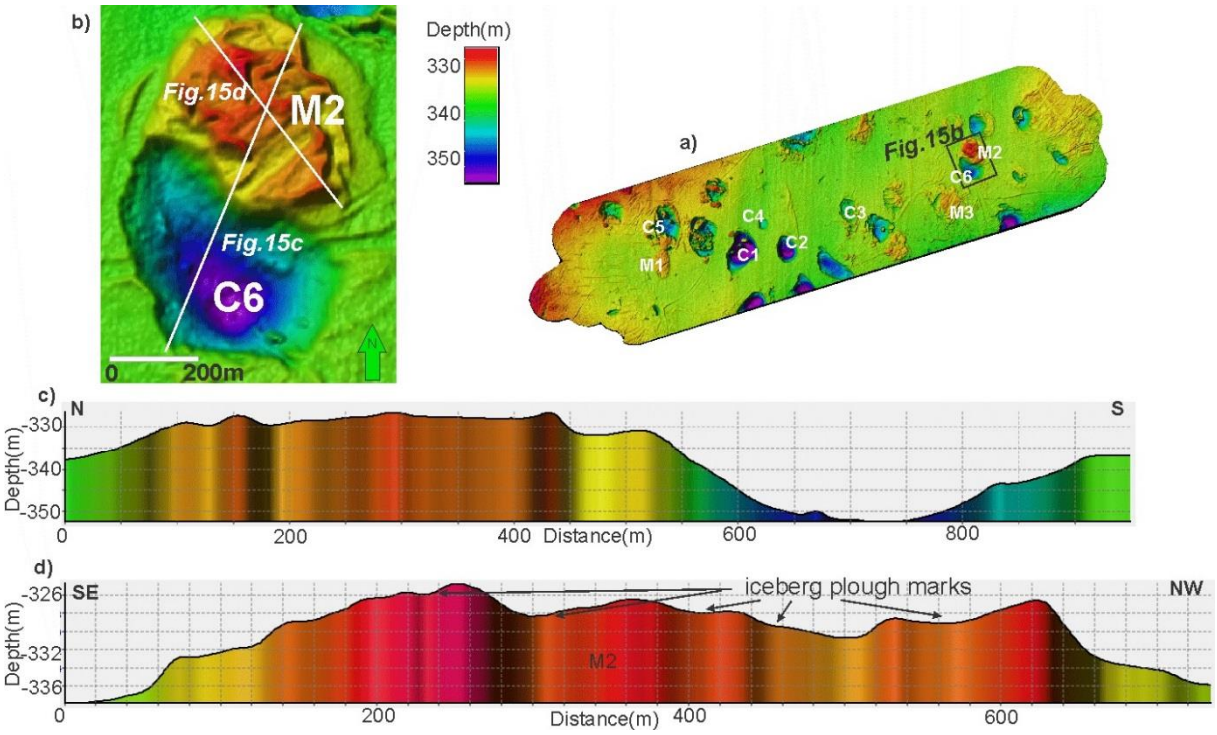

Figure 15. a) Bathymetry map indicating location of (b); b) Perspective image of crater C6 and mound M2; c) bathymetry profile across the whole structure C6-M2 with location indicated in (b); d) bathymetry profiles across the mound M1, with location indicated in (b).

Formation M2 has length and width of 580 m and 350 m, respectively, and maximal relief is 12 m. View from above gives strong impression that structure is composed of several ridges cause of significant relief variations. However, closer look on the bathymetry cross-section profile on Figure 15d makes it more probable for structure to be “one-piece” build-ups, although, roughly eroded by iceberg plough marks. Natural mound relief is enlarged by levees of iceberg scours forms highest peaks of the mounds.

Mound M3

Mound M3, shown on the Figure 16, have the same orientation and are rather similar with mound M2, based on their morphological characteristics and cross-section. Mound M3 is, however, more circular-shaped, and is 430 m wide and 470 m long, and rises up to 8 m over the surrounding seafloor.

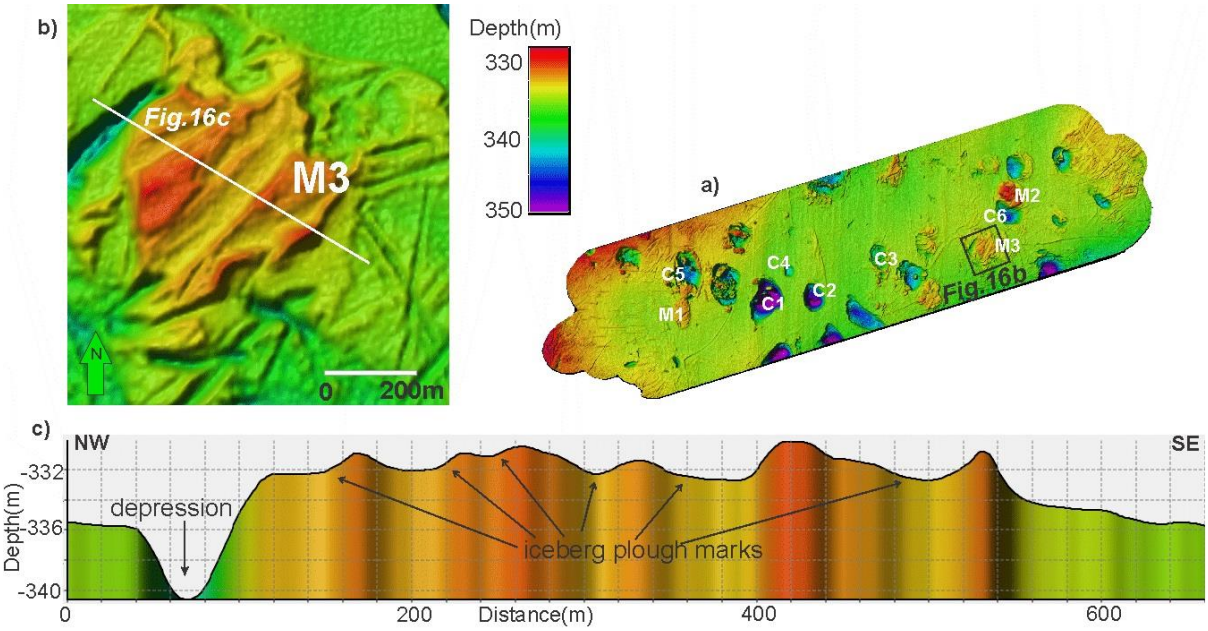

Figure 16. a) Bathymetry map indicating location of (b); b) Perspective image of mound M3; c) bathymetry profile across mound M3 with location indicated in (b).

Smaller craters

More than 20 smaller scale craters are spread around the area surveyed. They occur irregularly on the seabed both single, in groups and as satellites of the larger formations. Some craters are deeper and more sharply defined than others. On Figure 17a part of the seafloor is shown and seven such smaller craters are labelled in red circles and indicated by arrows. These structures are oval to circular in shape and have diameter of 30-40m and relief varying in range 0.5-2m. Figure 17b and Figure 17c represent bathymetry profiles across two of craters on the study area.

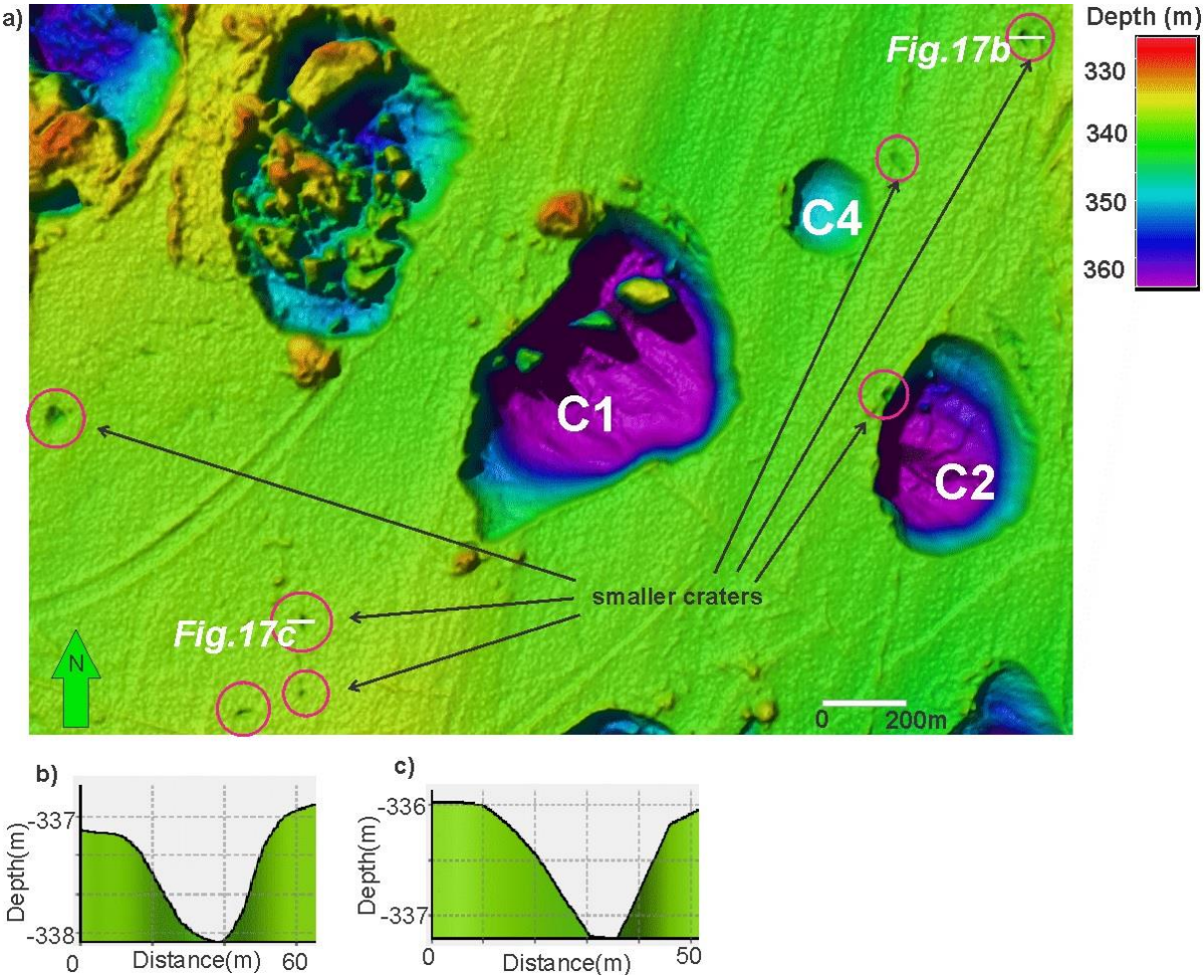

Figure 17. a) Bathymetry of the part of the seafloor in the study area, which location is demonstrated on Figure 9. Location of craters C1, C2 and C4 is indicated, smaller craters are concluded in red circle and marked by arrows; b and c) bathymetry profiles across particular craters, which location is indicated in (a).

8.2 Seismic interpretation

Faults

The study area at Upper Bjørnøyrenna is highly faulted. Fault system has been identified and interpreted from seismic profiles and variance maps preferably at depths from 485 to 550ms, which show different structural features dominant at different depths. Elongated structures on the variance maps are interpreted as faults and fractures and are identified in seismic profiles by reflection discontinuities. Faults have principle orientation in northwestern-southeastern direction with few exclusions, which corresponds to regional faulting from Permo-Triassic extension. Several cross-cutting faults are also presented. Figure 18 demonstrates variance maps and one of the seismic profiles across the study area used for fault interpretation.

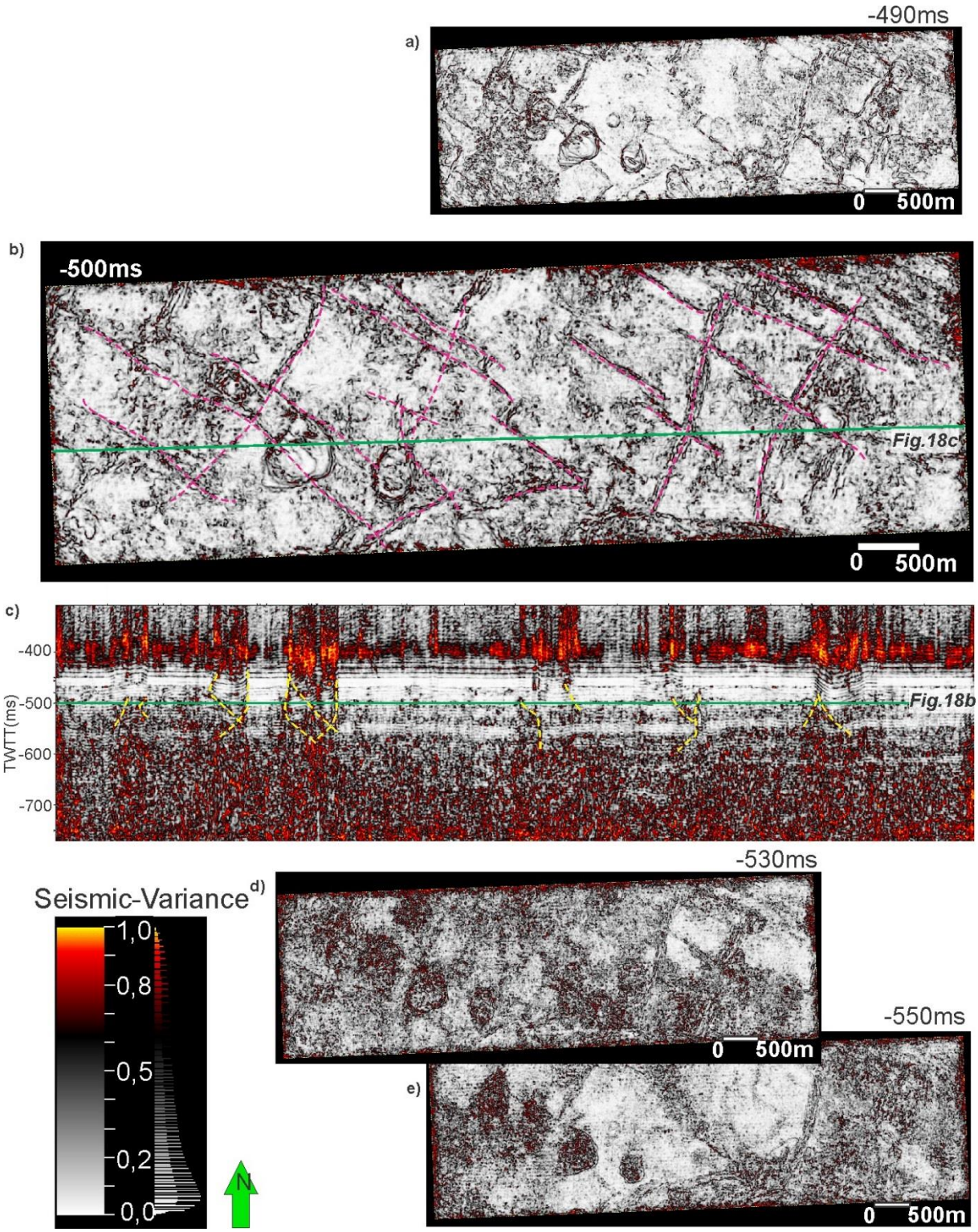

Figure 18. Variance maps in combination with seismic profile for identification and interpretation of faults within the study area. Legend and direction of the north arrow in left lower corner apply to all figures a-e: a, d, e) Variance maps at 490, 530 and 550 ms, respectively; b) Variance map at 500 ms. Dotted rose lines demonstrate proposed fault lines. Solid green line marks location of seismic profile shown in (c); c) seismic profile across the seafloor. Dotted yellow lines demonstrate proposed fault lines. Solid green line marks depth of 500 ms.

The seismic data (Figures 19-23) show also vertical and sub-vertical zones of distinct distorted seismic signals, which resembles chimneys and pipes or similar focused fluid-flow structures in the subsurface. Analysis of seismic profiles reveals that these acoustic anomalies occur mostly within fault zones, what leads to preposition that faults in the study area may represent vertical migration routes for shallow gas.

Focused fluid flow

Typical for fluid escape pipes and seismic chimneys in this study area are to have rather distinct vertical orientation with minor lateral offsets. These vertical columnar structures have diameters varying with depth. Gas pipes are identified on the majority of seismic profiles across the area surveyed, examples are shown on Figures 19 - 24. Presence of gas pipes has been revealed under all of the internal mounds inside the craters (Figure 20). Gas chimneys that represent larger vertical or sub-vertical areas of distorted seismic, than gas pipes, are not ubiquitous, but sufficiently common to be significant features as well. They are, in most occasions, found in association with depressions on the seafloor, as shown on the Figures 19b, 20. Unfortunately, cases when root zone can be identified with certainty are not observed on the seismic profiles along the area of interest. Limited penetration of the subsurface by the seismic waves due to relatively hard and shallow sandstone bedrock is enhanced by the loss of imaging accuracy and data quality with depth. Pipes are most clearly visible at depth between 460 – 550 ms, seismic chimneys are identified to a bit deeper levels of 625 ms. Reduced signal combined with high noise ratios makes it impossible to identify the true base of pipes and leaves the possibility for the root zone to be located at the deeper horizons. During the study of multiple seismic profiles form the study area, focused fluid flow structures were observed along straight paths following faults, what revels faults zones to be acting as vertical conduits. Although, the vast majority of fluid flow structures terminate at surface depressions and mounds, demonstrating a link between their formations through transport of methane, there are few gas pipes presented, terminating abruptly at a discrete subsurface horizon. One of examples is demonstrated on Figure 22. Such pipes may represent potentially important paths for venting methane directly to the seabed and are most probable associated with faults.

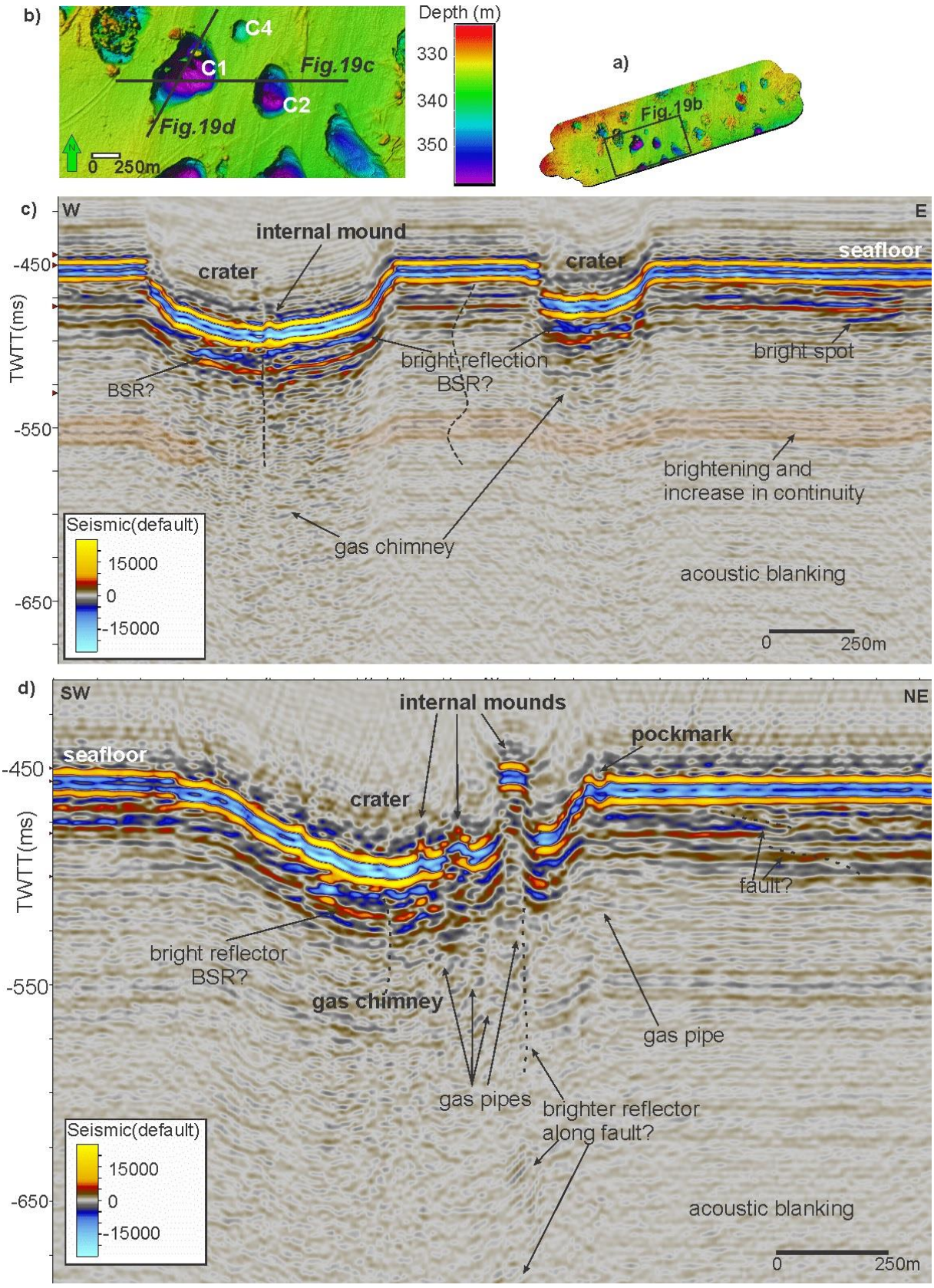

Figure 19. a) Bathymetry map indicating location of (b); b) Perspective image of the part of the seafloor indicated on (a). Location of the seismic profiles c and d is indicated by solid black lines; c and d) Seismic profiles across the seafloor. Location is indicated on (b). Seismic anomalies are named and indicated by arrows. Faults are marked by black dotted lines.

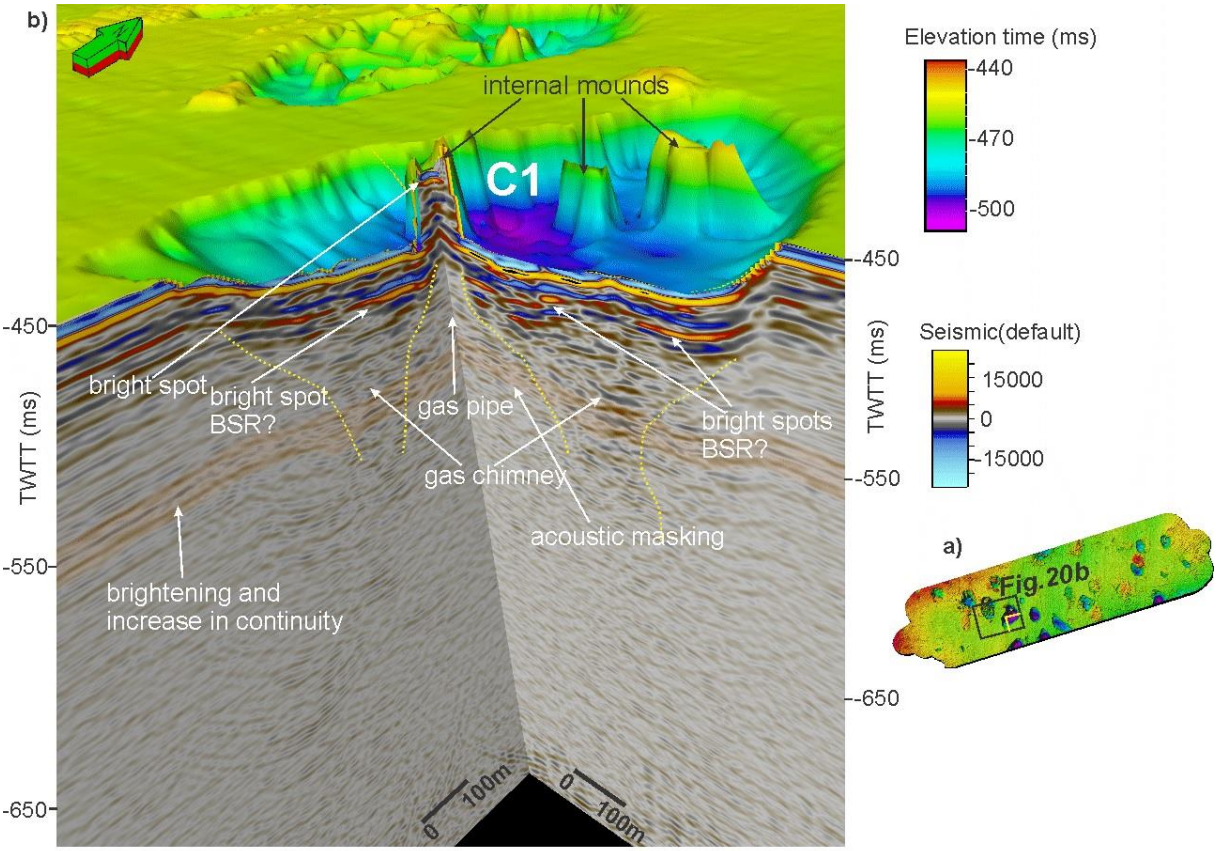

Figure 20. a) Bathymetry map indicating location of (b) by black rectangle. Two solid yellow lines inside the rectangle indicate location of seismic sections; b) 3D view of time-structure map of the seafloor and associated crater C1 accompanied by two seismic sections through crater C1. Seismic anomalies are named and indicated by arrows. Approximate boundaries of gas chimneys are marked by yellow dotted lines.

High amplitude anomalies

Strong seafloor amplitudes are accompanied by the local occurrence of moderate to high amplitude anomalies that generally correlate with location of depressions and mounds and may suggest the presence of hardgrounds, carbonates, free gas or methane hydrates. Most of the high amplitude reflections are observed in association with gas chimneys and along faults what may be caused by fluid migrating vertically through them and by high gas content in the porous infill. These features indicated by arrows on Figures 19-24 and its noted that brightness of observed anomalies vary significantly. Bright spots observed under depressions within the study area are interpreted to be parts of bottom simulating reflector, which is discussed in the next indent. At depth of 550 ms seismic reflector with increased brightness and continuity is defined on the most of seismic profiles from the study area (Figures 19c, 20, 21c, 23, 24) and interpreted to represent a lithological change to a denser layer.

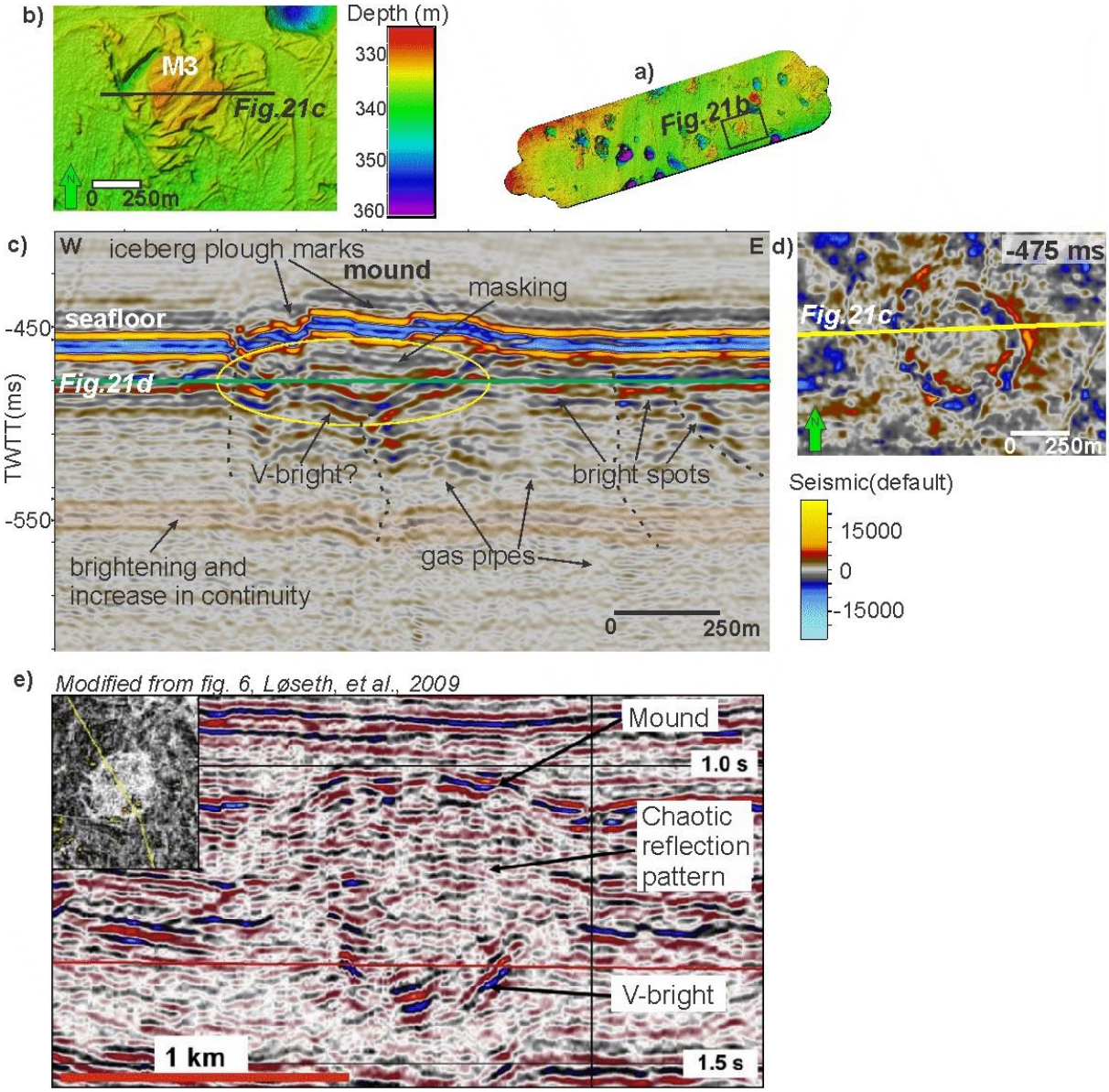

Figure 21. a) Bathymetry map indicating location of (b); b) Perspective image of the part of the seafloor indicated on (a). Location of the seismic profiles c is indicated by solid black line; c) Seismic profiles across the seafloor. Location is indicated on (b). Seismic anomalies are named and indicated by arrows. Faults are marked by black dotted lines. Anomaly in question is concluded in yellow circle; d) Time-slice at 475 ms. Location of seismic profile (c) is indicated by yellow solid line; e) Vertical seismic section representing chaotic reflection zone with mound as upper boundary and V-bright as lower boundary. The chaotic reflection is interpreted as mud and sand and the high-amplitude V-bright as a carbonate-cemented sand injection. Modified from Løseth et al. (2009), fig. 6.

On the few seismic profiles, other forms of high amplitude anomalies are observed. One of the most prominent of them is demonstrated on the Figure 21c and represents an individual bright

reflector beneath one of the mounds bend downwards. Time slice at 475 ms through the seismic profile (Figure 21d) reveals circular-shaped structure with high amplitude at the rim surrounding area of wipe-out seismic. Several explanations has been considered, most probable of which are paleo-pockmark on which place the mound was formed and V-bright observed below chaotic reflection zone, interpreted as mud and sand, and representing carbonate-cemented sand injection structure, similar to one described by Løseth et al., 2009 (Figure 21e).

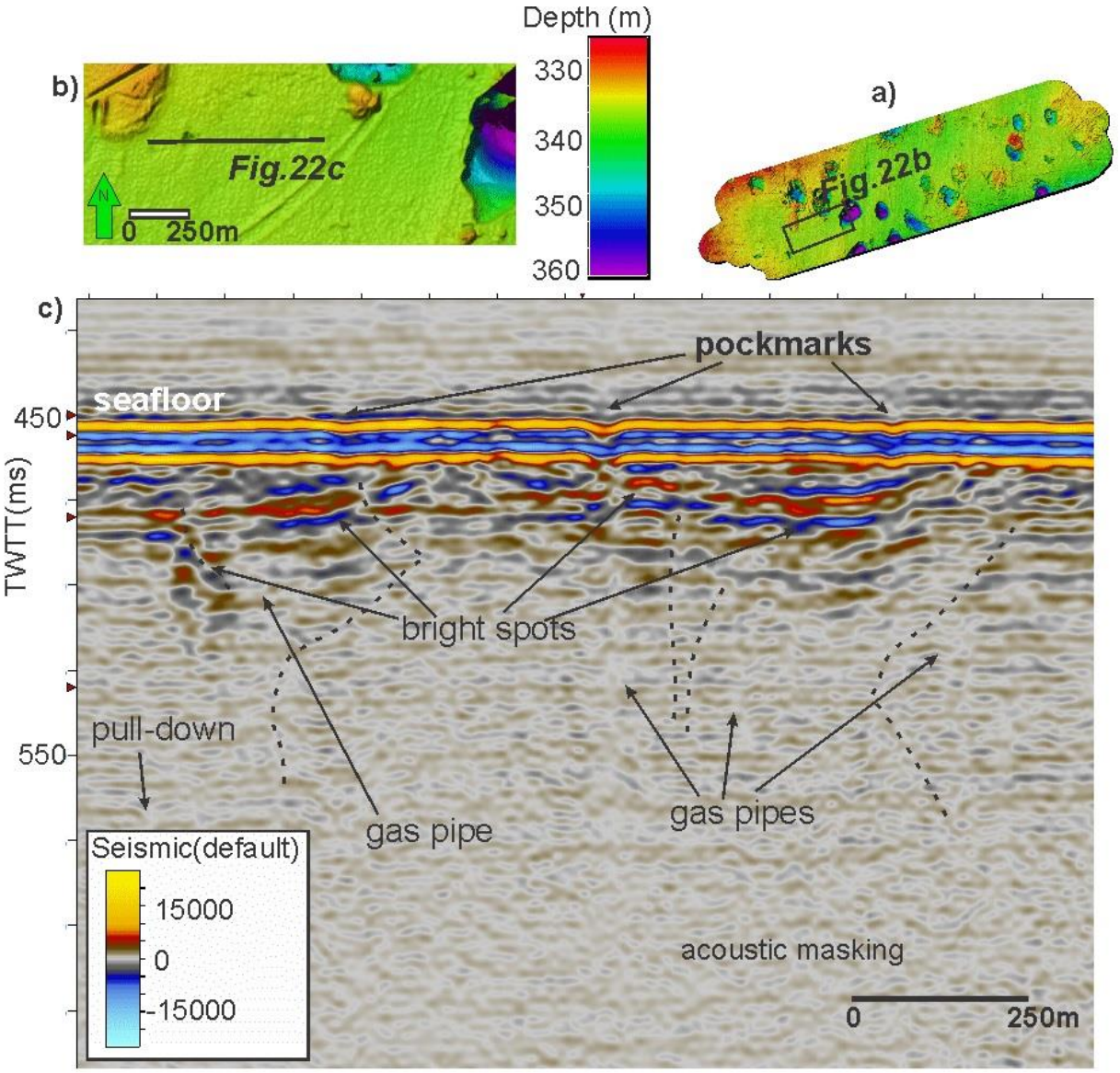

Figure 22. a) Bathymetry map indicating location of (b); b) Perspective image of the part of the seafloor indicated on (a). Location of the seismic profile c is indicated by solid black line; c) Seismic profile across the seafloor. Location is indicated on (b). Seismic anomalies are named and indicated by arrows. Faults are marked by black dotted lines.

Bottom simulating reflector

In the study area, the presence of strong reflector with reserved polarity, commonly accompanied by sudden blanking of the reflection, are compared with gas hydrate-related bottom simulating reflector (BSR). The BSR is revealed in shallow subsurface underneath the most of depressions, at depth between 25 - 75 ms bsf, roughly mimicking seafloor reflector. However, its appearance is rather irregular and highly disturbed by acoustic masking zones. The occurrence of such discontinuous BSR may represent gas accumulations below hydrate stability zone within highly fractured fault zones. The BSR is marked on Figures 19, 20, 23 and Figure 24 and insets on the Figure 23c demonstrate phase and polarity of the probable BSR in comparison to the seafloor reflector. However, more detailed analysis is required to make certain conclusions.

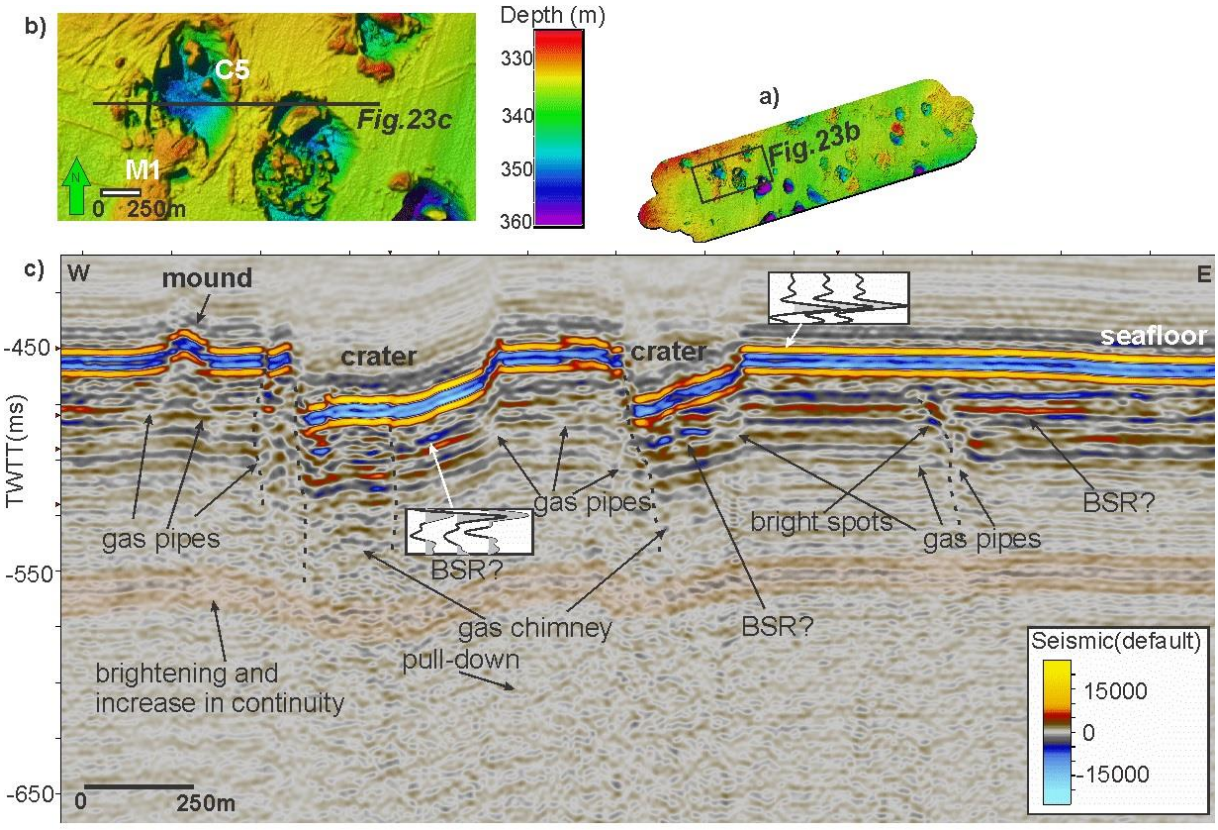

Figure 23. a) Bathymetry map indicating location of (b); b) Perspective image of part of the seafloor, with crater C5 and mound M1. Location of seismic profile (c) is indicated by solid black line; c) Seismic profile across the seafloor with location indicated on (b). Seismic anomalies are named and indicated by black arrows. Faults are marked by dotted black lines. Two small insets on the seismic profile indicated by white arrows show variable area/wiggle trace displays of a BSR (negative phase) and of the seafloor reflection (positive phase).

Velocity anomalies

Presence of gas within sediments reduces seismic wave velocity and pull-down effect (smile) is created on the underlying reflector. This feature is observed on a few seismic profiles across the area and is marked on Figures 22 and 23.

Acoustic blanking

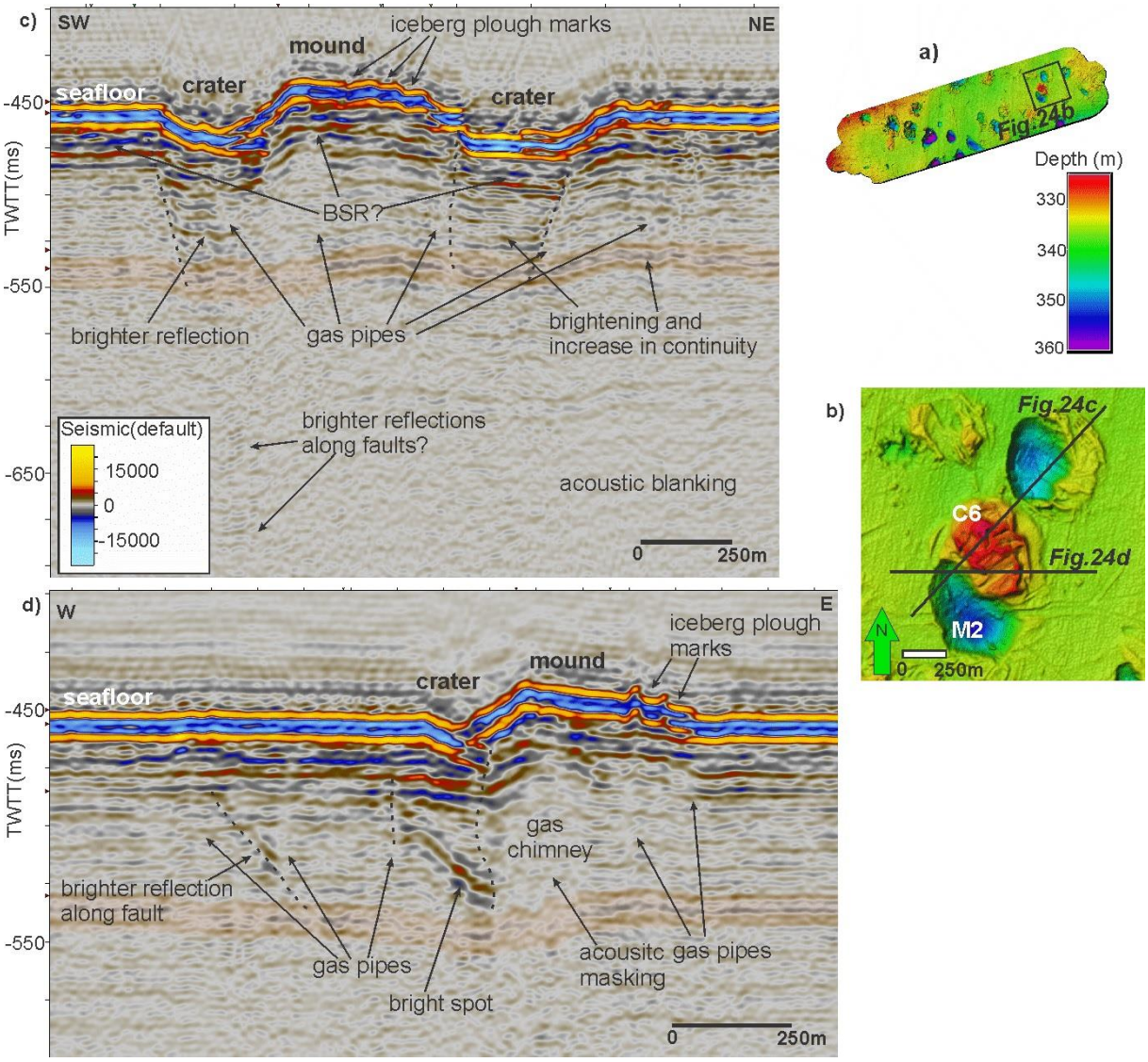

Figure 24. a) Bathymetry map indicating location of (b); b) Perspective image of part of the seafloor, with crater C6 and mound M2. Location of seismic profiles (c) and (d) is indicated by solid black lines; c, d) Seismic profiles across the seafloor with location indicated on (b). Seismic anomalies are named and indicated by black arrows. Faults are marked by dotted black lines.

In the study area, acoustic blanking in sediments is observed on the most of seismic profiles across the study area. Such anomaly in most occasions is observed at depth below 650 ms and within gas chimney where seismic reflection is highly distorted. Both cases is demonstrated on Figure 24c and 24d, respectively. It is interpreted to be caused by both disturbance of seismic wave in gas-charged sediments and reflection of a large proportion of acoustic energy by an overlying quite hard Triassic sandstone bedrock, reducing returning signal.

8.3 Gas in water column

The Upper Bjørnøyrenna in the central Barents Sea is an area with gas venting from a seabed. During analysis of backscattered data provided by 18 kHz echo sounder, 749 water column anomalies, which correspond to gas plume, have been identified during the investigation. Each of flares has been assigned a quality factor from 1 to 9 dependent on the set of qualities based on reflection strength, continuity and start point, in the study area. There has not been made chemical analysis of gas bubbles from plums but they most likely contain methane as the net flux of methane from the area of the Barents Sea only few kilometers away from the study area and with the same morphological features investigated by Solheim et al. (1993) and Lammers et al. (199) was estimated to be about 2.9×10^4 g CH4 km $^{-2}$ yr^{-1} and vertical profile revealed extremely high methane content in range between 29.0 to 56.7 nM. (Lammers et al., 1995; Solheim et al., 1993)

8.3.1 Gas flare classification

Each single flare was assigned a subjective quality factor from 1 to 9 corresponding to combination of qualities such as strength, continuance and start point (Table 1). Quality factor 1 to 8 was assigned to gas seepages that more or less corresponded to the qualities of interest. Estimations were made the following way:

- Continuity: gas plumes with uninterrupted length equal or greater than 50 m were considered “long”. Shorter than 50 m were interpreted as “short”.
- Strength: flares which are visually perceived to be colored red more than yellowish or greenish when the target strength (Ts) histogram has range between 75 and 45 negative dB are interpreted to be “strong”. Others are considered to be “weak”.
- Start point: difference between the seepages that go directly from the seafloor and the flares that start in midwater and are most likely to be a part of some bottom-plume but we cannot be sure which exactly.

After discussion, quality factor 9 was added to be used for classification of gas seepages which relation to quality factors 1 to 8 is uncertain because of variable features. There are mostly flares with uneven strength or discontinuous flares.

Figure 25 represents the examples of along trackline echogram profile of water column backscattered data. Anomalies, red to green, in the black rectangles A and H on Figure 25a and I on Figure 25b are considered noise and excluded from qualification. Water column anomalies marked by black spheres B-G (Figure 25a) are all considered gas plumes remarkable enough to be reflected in the classification. The same principle of visual identification of gas seepages were applied to all other echogram profiles.

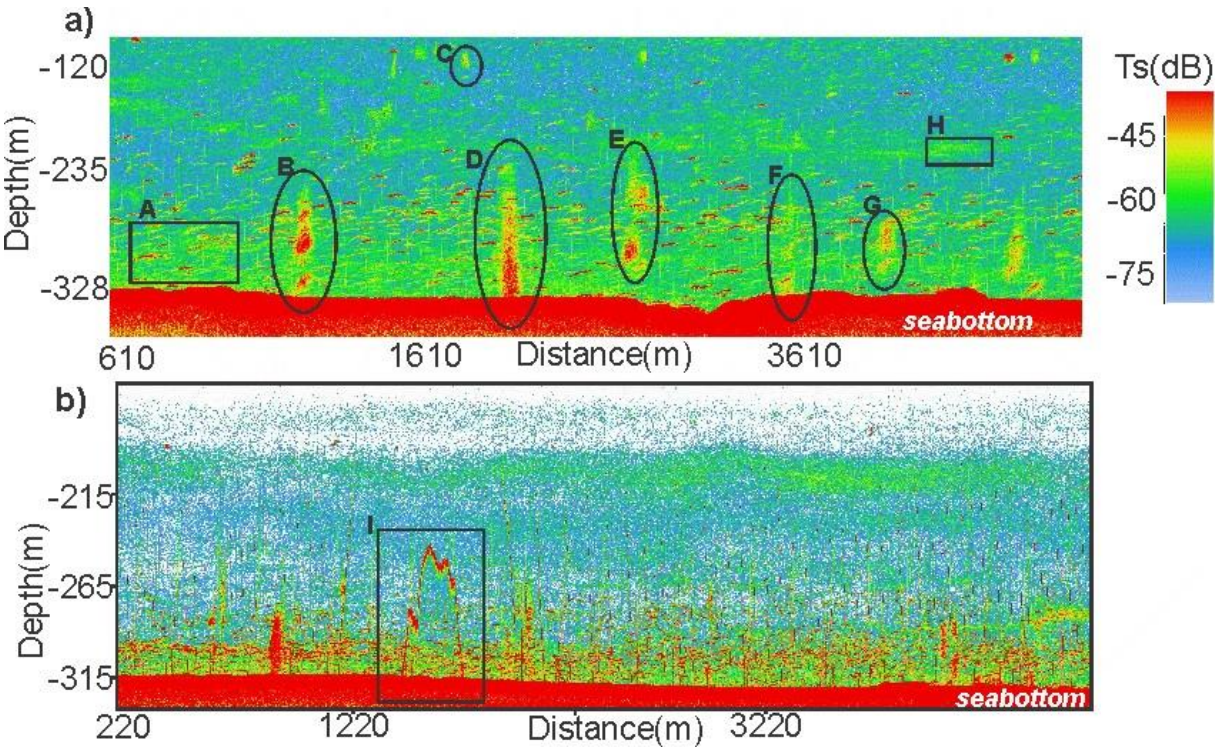

Figure 25. Examples of along trackline echogram profiles of water column backscattered data; a) Water column anomalies marked A and H are classified as noise and B-G as gas plumes; b) Anomaly I in the black rectangle is considered noise.

Following Table 1 demonstrates how combinations of qualities correspond to quality factors of gas plumes:

	Continuity	Strength	Start point
Quality factor 1	Long	Strong	From seabed
Quality factor 2	Short	Strong	From seabed
Quality factor 3	Long	Weak	From seabed
Quality factor 4	Short	Weak	From seabed
Quality factor 5	Long	Strong	In midwater
Quality factor 6	Short	Strong	In midwater
Quality factor 7	Long	Weak	In midwater
Quality factor 8	Short	Weak	In midwater
Quality factor 9	Variable features		

Table 1. Combination of qualities of interest correspondingly to quality factors 1 to 9.

8.3.2 Results

Figure 26 shows examples of gas flares assigned to each quality factor from 1 to 9. Quality factor 9 is represented by three images: Figures 26i, j, k shows different types of flares with variable features as discontinuity, uneven strength and external disturbance causing difficulties with identification of a flare, respectively.

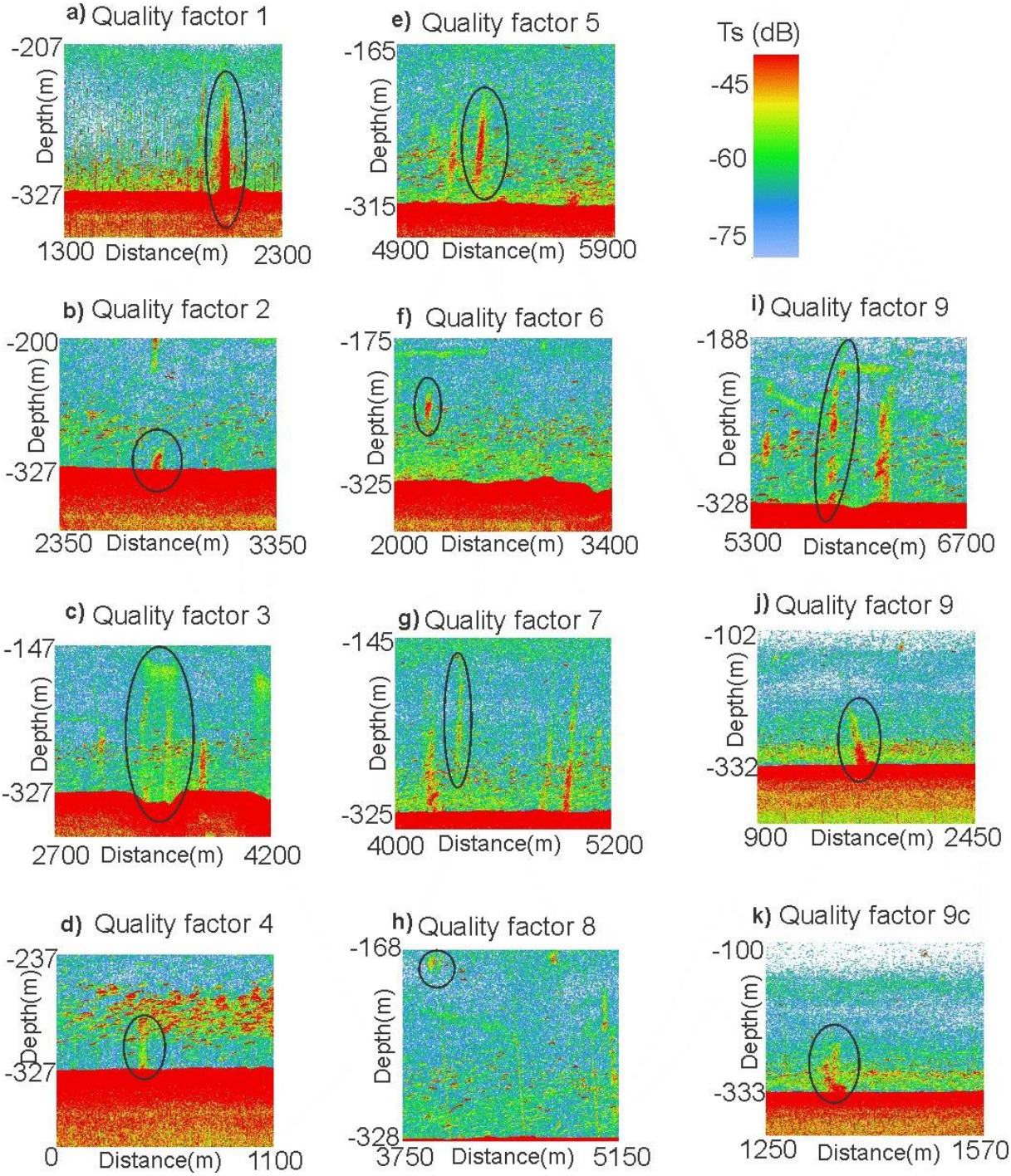

Figure 26. Example of gas flares from water column backscattered data from the Upper Bjørnøyrenna in the central Barents Sea assigned to quality factors 1 to 9. Gas plum of interest for each quality factor is concluded in the black circle. Legend target strength (dB) in the higher right corner applies to all of the images a – k;.a) Quality factor 1; b) Quality factor 2; c) Quality factor 3; d) Quality factor 4; e) Quality factor 5; f) Quality factor 6; g) Quality factor 7; h) Quality factor 8; Quality factor 9 is represented by several images: (i): discontinuous flare; (j): uneven reflection strength; (k): disturbance in the water column causing difficulties to classify gas flare with confidence.

When mapping and classification of gas seepages in the study area were completed, models shown below on Figure 27 were compiled. Images from (a) to (d), in alphabetic order, represents the bathymetry of Upper Bjørnøyrenna with mapped gas plums of one particular quality factor 1, 2, 3 and 4, respectively. Gas flares of quality factors 1 and 2 represent strong reflections directly from the sea bottom and form nearly the largest groups. They are almost evenly spread in east-west direction but with highest concentration of plums in the eastern end of the study area. Weak reflections assigned with quality factors 3 and 4 are going from the seabed and are densest in the western central part of the area of investigation. Their presence are easily associated with deep depressions and are possibly caused by small-scale and/or periodical gas leakage, which changes methane-flux in water column. More data and prolonged investigations are needed to discuss causes and changes in seepages. Flares in the midwater (quality factors 5 - 8) are parts of some bottom flares divided from it and are shown on the Figure 27f. They are traveling in the water column and are presented along all of the zigzag-pattern where gas is leaking from the subsurface. Flares with variable features (quality factor 9) are demonstrated on Figure 27e, some of them starts from the seabed and some are midwater plums. Table 2 provides information about quantity distribution of gas flares between quality factors 1 to 9. Note, that because of classification's subjective nature, some of the gas flares might be missed or mixed up.

	Quantity of gas flares (stk.)
Quality factor 1	124
Quality factor 2	102
Quality factor 3	29
Quality factor 4	29
Quality factor 5	68
Quality factor 6	136
Quality factor 7	88
Quality factor 8	118
Quality factor 9	55
Total	**749**

Table 2. Quantity distribution of gas flares between quality factors 1 to 9

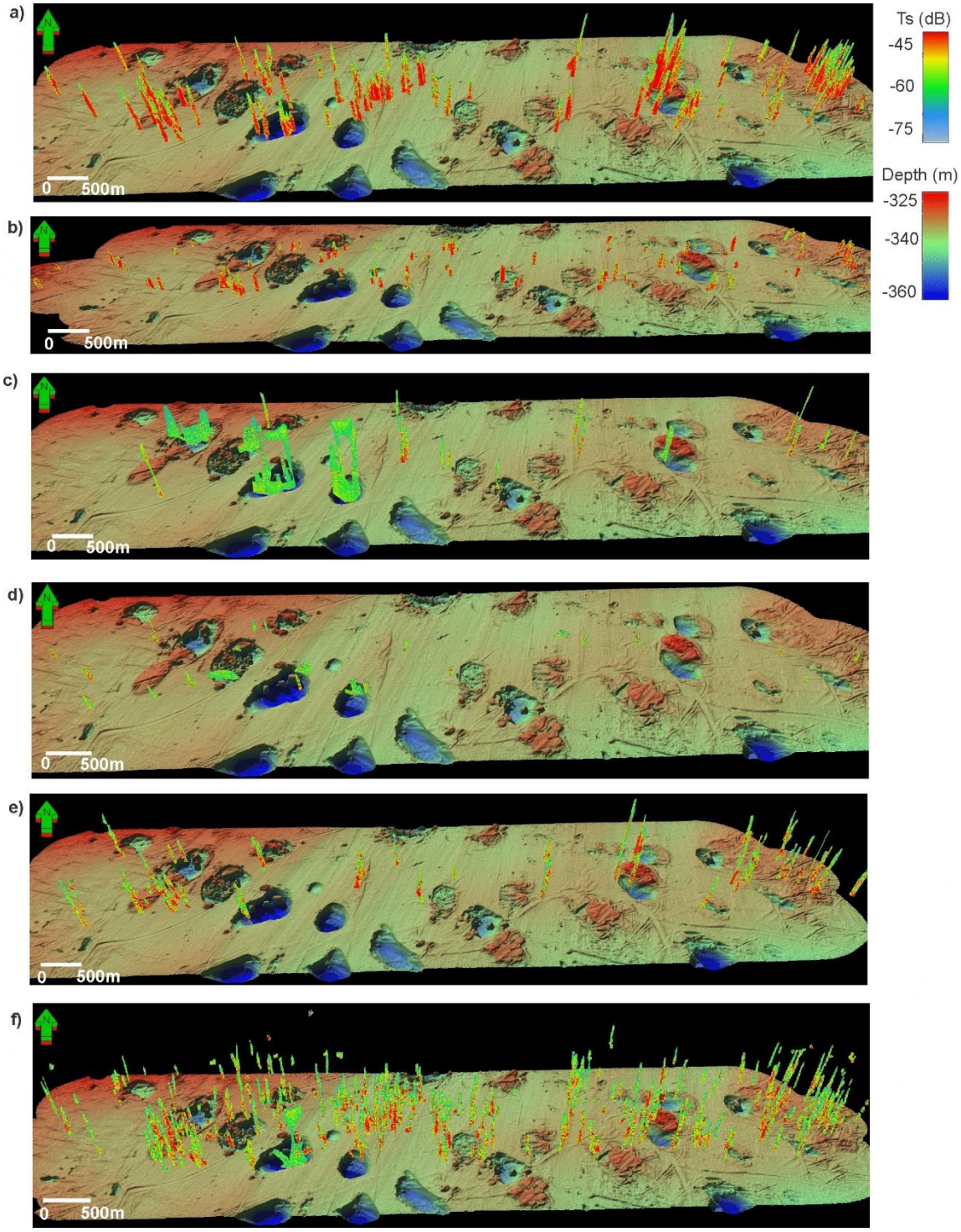

Figure 27. Bathymetry map of the study area in Upper Bjørnøyrenna with mapped gas flares of quality factors 1-9. Legends in the right upper corner show target strength (Ts) of gas flares in dB and bathymetry depth in meters. Both legends and north arrow apply to all of the images (a)-(e): a) Bathymetry map of the study area with gas flares of quality factor 1; b) Bathymetry map of the study area with gas flares of quality factor 2; c) Bathymetry map of the study area with gas flares of quality factor 3; d) Bathymetry map of the study area with gas flares of quality factor 4; e) Bathymetry map of the study area with gas flares of quality factor 9; f) Bathymetry map of the study area with gas flares of quality factor 5,6,7 and 8, all in midwater.

Figure 28a shows all 749 gas flares, which have been identified and mapped on bathymetry map of the Upper Bjørnøyrenna. Gas seepages form an irregular pattern on the seafloor and are most dense in the Eastern end of the study area and in the central cratered part and became fewer closer to the uplifted Western part. Only the gas plumes going directly from the seabed, what includes flares of quality factors 1-4 and partly factor 9, are presented on Figure 28b to demonstrate pattern of real leakage. Deeper investigations and re-survey are required to make reliable assumptions about local variations of seep activity.

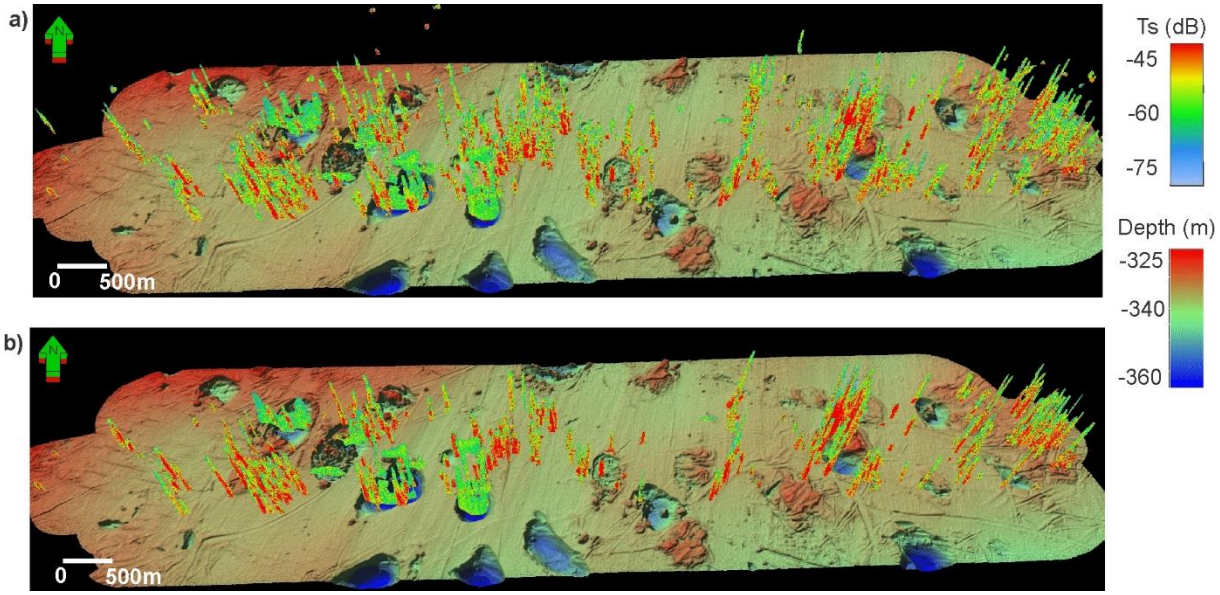

Figure 28. a) Bathymetry map of the study area in Upper Bjørnøyrenna with all identified gas flares mapped; b) Bathymetry map of the study area with mapped gas flares going directly from the seabed.

8.4 Interpretation of craters and mounds

The fault system, identified from the seismic data, and gas plumes directly from the seabed, show similar pattern of distribution, a correlation, which is considered unlikely to be random. Therefore, faults are interpreted to be active migration routes for the gas leaking from the subsurface. Figure 29 represent the bathymetry map of the area of interest, where faults and exit points of gas flares on the surface are marked. In addition, detailed seismic interpretation shows clear correlation between seismic amplitude anomalies, BSR and distinct craters and mounds on the seafloor. Based on overall analysis of seismic and echo sounder data from the area survey, the following were suggested: formation of craters and mounds has occurred, largely, as a result of gas hydrates formation and decomposition in shallow subsurface, supplemented by continuous supply of the gas-saturated pore fluid migrating through fractured fault zones from deeper reservoir. Therefore, craters and mounds in the study area are interpreted to

represent a result of the process of formation and decomposition of gas hydrate in shallow subsurface, described in detail in paragraph 8.5 and illustrated on Figure 30. Prominent craters C1, C2, C4 - C6 and other, similar to them, may be referred to as collapse depressions caused by gas hydrate decomposition and pore pressure build up. Mounds on the seafloor, including M1, M2 and M3, are interpreted to be collapsed pingo structures. Structure C3 (Figures 12) because of low relief may be referred to as both collapse depression and collapsed pingo. Location of all structures mentioned in the text is marked on Figures 9 and 29.

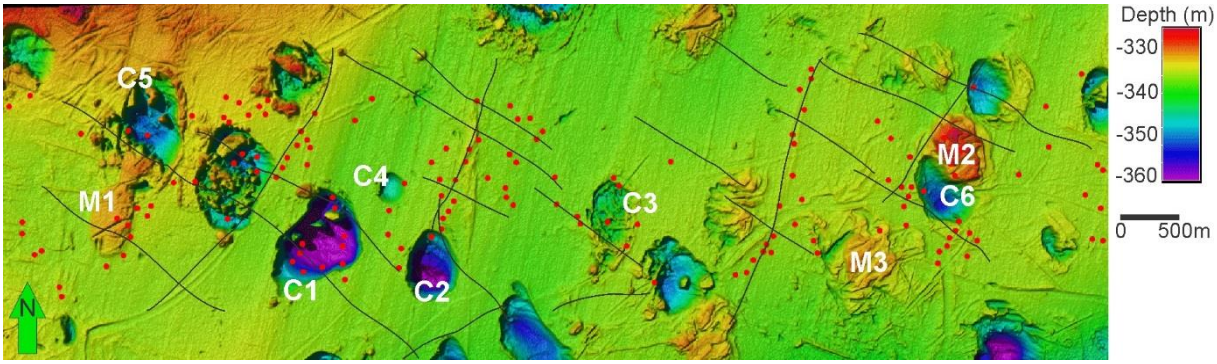

Figure 29. Bathymetry map of the part of Upper Bjørnøyrenna. Black lines mark faults and red dots demonstrate distribution of gas plumes going directly from the seabed. Craters C1-C6 and mounds M1-M3 are marked.

Smaller craters, shown on Figure 17a, are interpreted to be pockmarks. These features were for the first time mentioned by King et al. (1970), who suggested them to be formed by ascending gas or water. Seismic profiles (Figure 22) from the study area show direct correlation between seismic anomalies (gas pipes) and distribution of the described features within the seabed. These small craters are considered to "record the existence of seepage" and be formed by the removal of material by fluid and gas escaping from the sediment. (Hovland et al., 1988)

8.5 Formation model

The formation mechanism of craters and mounds on the seafloor within the study area in the Upper Bjørnøyrenna, interpreted to be a function of gas hydrate formation and decomposition is schematically presented on Figure 30 according to the following six phases:

1) Gas hydrate nucleation within the Triassic rocks beneath the ice during the last glaciation due to upward migration of gas-saturated pore fluid and free gas from deeper reservoir through existing fault system.

2) Gas hydrate growth results in expansion of volume, which is accompanied by uplift and deformation of upper sedimentary layers.

3) During the deglaciation, gas hydrates became gradually depressurized what leads to them been unstable and melt. Decomposing of methane hydrate causes increase in required storage volume by factor at least six, according to Hovland et al., 1988. At the same time, continuing supply of pore fluid saturated with gas from underlying levels builds up excess pore pressure. Excess pore pressure and growth of gas hydrate is revealed by further deformation of the seabed, forming dome structure named gas hydrate pingo.

4) Excess pore pressure in the dome structure, after it has been lost its holding strength, is released by eruption through the fractures in the dome. Gas, water and sediment are ejected in the water column.

5) Gas hydrate pingo structure collapses forming variable structures such as collapse depressions and collapsed pingoes as a consequence of hydrate decomposition and pore pressure.

6) Stabilization of gas hydrate. Fault zone and fractures in the gas hydrate layer are still working as leakage routes for gas from underlying levels.

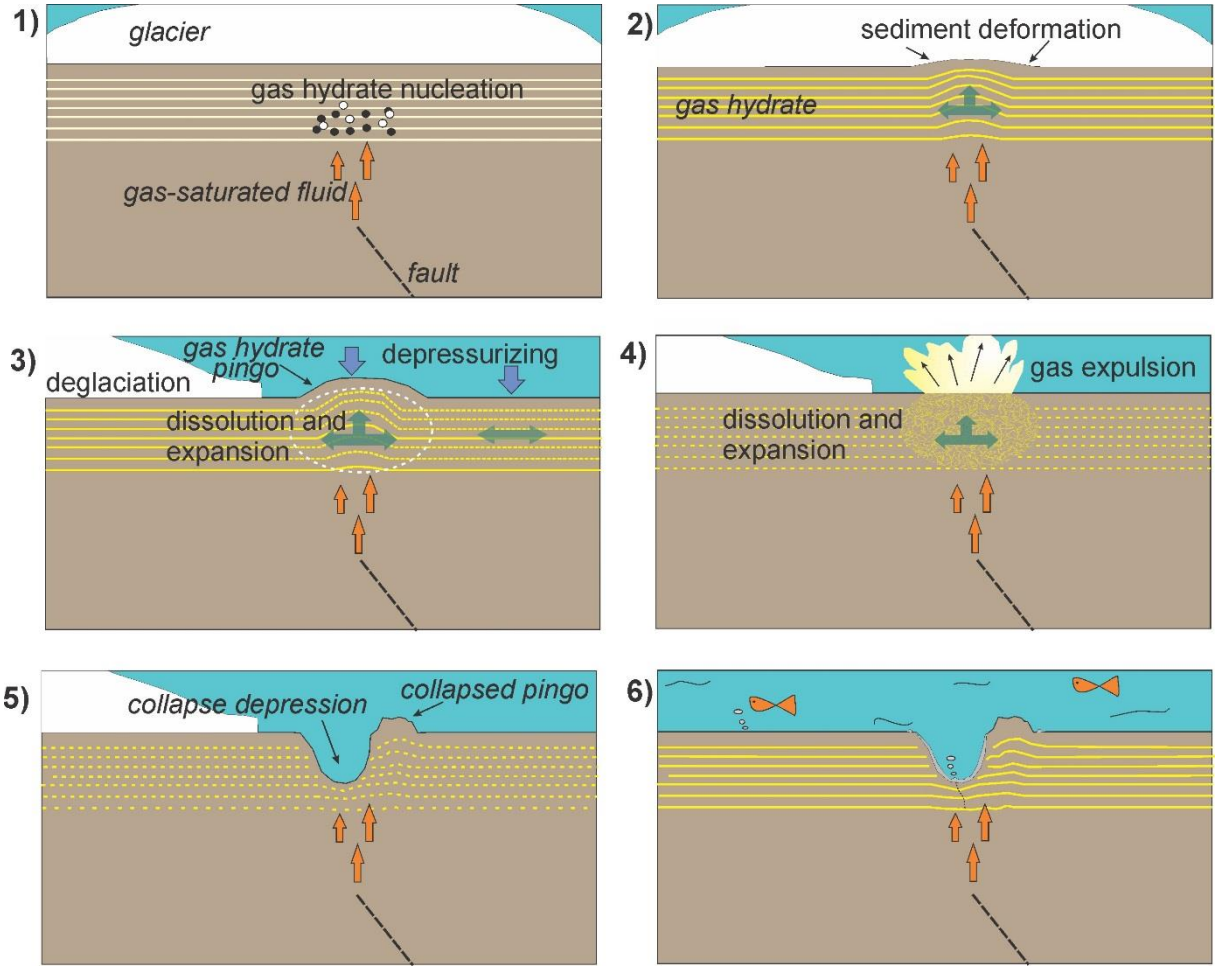

Figure 30. A conceptual sketch showing formation model for craters in the Upper Bjørnøyrenna, the central Barents Sea. 1) Gas hydrates nucleation due to upward migration of gas-saturated pore fluid; 2) Growth of gas hydrates leads to deformation of upper sedimentary layers; 3) Gas hydrates are depressurized during deglaciation and became unstable and melt what leads to increase in required storage volume and further expansion. Gas-saturated pore fluid continues to supply and builds up excess pore pressure. Gas hydrate pingo is being formed; 4) Expulsion of the gas, water and sediments in the water; 5) Collapse of dome structure forming collapse depression or/and collapsed pingo; 6) Stabilization of gas hydrates, leaving depression and collapsed pingo on the seafloor. Gas from subsurface continues to leak through fault zone and fractures.

9. Discussion

Several researches have been previously made in the study area. Solheim et al. (1993), as well as Long et al. (1998), studying the area of the Upper Bjørnøyrenna, mention that seafloor in this part of the Barents Sea is characterized by a fields of large semicircular closed depressions (Figure 31). Data from hydrosweep survey in 1991 proclaimed also presence of the several mounds 5- 10 m high near the craters, but these formations were misinterpreted to represent an artefact in data acquisition due to cross-talk. However, later data proved mounds within the craters to be real geomorphological structures and initiated discussions about their potential origin as well as crater formation mechanisms. (Long et al., 1998; Solheim et al., 1993)

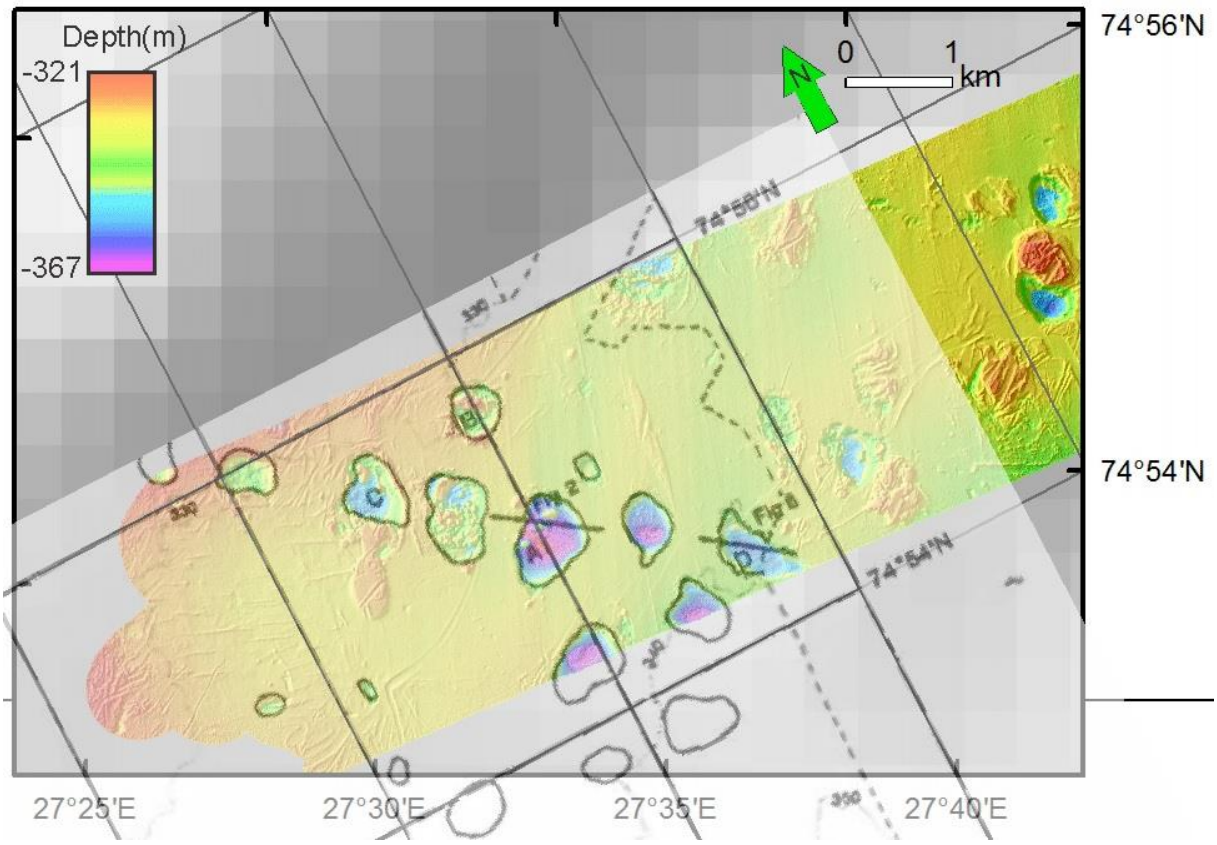

Figure 31. Bathymetry map of the part of the study area in Upper Bjørnøyrenna provided by multi-beam echo sounder during survey in June 2015 underlying the 50% transparent elevation map of the same area compiled by Long, et al. (1998), based on the hydrosweep surveys from 1991 and 1993. Modified from Long et al. (1998), fig. 1.

General understanding of glaciation history of the Barents Sea as well as identification of the glacial structures on the seabed within the study area suggests that this part of the Barents Sea has been covered by the ice sheet during the Late Weichselian Maximum and is confirmed by

Solheim et al. (1993) and Winsborrow et al. (2009). Pre-Late Weichselian age for the described crater and mound structures, assuming that they are a result of the same process and were formed simultaneously, seems unlikely. Pronounced and distinct patterns inside the depressions suggests that they were not filled with glacial sediments during glaciation, otherwise, it would be expected for them to be smoothed and infilled with time and demonstrate partly buried pattern. Hence, preposition was made that craters and mounds in the study area were formed during the deglaciation period, around 15 cal ka BP, while the area were rather unstable. (Solheim et al., 1993; Winsborrow et al., 2009)

Mounds in the study area are characterized by an absence of basal structure corresponding to regional seafloor reflector (Figure 24), what makes them unlikely to be depositional structures. According to Serié et al. (2012), mounds without a basal paleoseafloor reflection "could result from intrusion of fluidized sediments or gas hydrate expansion in the shallow subsurface forming hydrate pingoes". Lack of extrusive features such as mud diapirs suggests against interpretation of mounds as a result of extrusive processes forming mud mounds or mud volcanoes. Otherwise, the presence of deeper reservoir and related developed fault zone as well as continuous active gas leakage confirms the high fluid flux from thermogenic origin in the study area over a prolonged time, keeping the methane concentration at the necessary level. This fact, together with the morphological characteristics of the mounds with absence of internal structures and basal reflection, their close association with BSR and seismic anomalies, supports the interpretation of the mounds in the study area as gas hydrate pingoes and makes them rather similar to structures from the Kwanza Basin, offshore Angola, described by Serié et al. (2012). (Serié et al., 2012; Hovland et al., 2006)

Solheim et al., 1993, considering shape and size of individual depressions in Upper Bjørnøyrenna, have discussed several possible mechanisms of their formation: meteorite impact, glacitectonic processes and processes related to shallow gas and gas hydrates in the area. (Solheim et al., 1993) These hypotheses were reconsidered with relevance to the depressions and mounds within the study area of Upper Bjørnøyrenna and contemporary data were taken into account. No survey and sampling provided since 1993 gave information, which could confirm the impact origin, like abundant impact metamorphic rocks or typical shock-related structures. Some structures observed within the study area (Figure 15) meet the morphological description of "hill-hole pair", which is the one of the most representative types of glacitectonic landforms consisting of a basic combination of "ice-scooped basin and ice-shoved hill". (Aber et al., 1989) However, "hill-hole pair" formation is a direct result of movement of glacier along seabed, during which some material is removed from up-glacier

basin and deposited as ice moraine. This not corresponds with observation that mounds in the study area lack basal paleoseafloor reflector. Although, "holes", in some cases, are identified, without "hills" in close proximity, the glacitectonic origin of the craters in the study area are still found unlikely. (Bluemle et al., 1984) Size of the depressions and suggested absence of the strong coupling between the glacier and its bed through freezing makes it doubtful for the glacitectonic processes to occur in the area. (Solheim et al., 1993) Active gas seepage in the study and presence of the numerous pockmarks within the study area confirms that gas is escaping through the seafloor and suggests eruptions. However, very vigorous gas eruption is required to create craters, which average diameter exceeds 400 m, in the rather hard Triassic bedrock. The origin of the mounds in the study area, interpreted to be collapsed gas hydrate pingoes suggests the possible influence of the processes of gas hydrates decomposition on the craters formation within the investigated area. It has been suggested that formation of the deep crater-like structures on the bottom of the central Barents Sea are most likely to be caused by eruptions of gas, when a large volume of free gas were released from the decomposition of gas hydrates during rapid deglaciation. (Solheim et al., 1993) Sultan, et al. (2010) introduced tentative model of the formation of collapse depressions in Niger delta as a function of hydrate formation and dissolution, which cause sediment collapse. He suggested five formation phases including free gas and gas hydrate nucleation above a critical depth; expansion of volume due to hydrate growth; decrease in gas content below saturation at the gas hydrate boundary due to decrease in fluid migration; hydrate dissolution and collapse; disappearance of the solid hydrate and the cease of fluid activities. Prior et al. (1982) and Hovland et al. (1988) also described pockmark-like features as collapse depressions in their studies and claimed them to be produced not because of erosion, but by the collapse of seabed when reduction of volume in "sediment-pore water-gas system" has occurred. Although, they did not make certain connections with gas hydrates, it would not interfere the main principal of the formation.

Proposed formation model, demonstrated in the paragraph 8.5, is a hypothesis, which is compiled based only on the analysis of seismic- and echo sounder data from the area surveyed. However, due to rather limited understanding of gas hydrate pingoes formation process, untypical morphometrical characteristics of the studied structures and subjective character of the current investigation, further data analysis and detailed discussions are required to make a conclusion about concepts viability.

10. Summary and conclusion

Seismic and bathymetry data from area surveyed in the Upper Bjørnøyrenna, the central Barents Sea, confirmed presence of the deep crater-like depressions and rough, uneven mounds within the seabed, reported by the number of previous investigations. Analysis of seismic and echo sounder data reveals clear connection between these distinct crater and mound structures on the seafloor and high amplitude anomalies, fluid flow anomalies and strong discontinuous BSR. From the echo sounder data 749 gas flares have been identified during the investigation, each of which has been assigned with quality factor from 1 to 9 dependent on the set of qualities as reflection strength, continuity and start point. Distribution pattern of the gas seepages correspond to the location of faults in the study area what suggest that gas is of thermogenic origin and is migrating from the deeper reservoir through porous layers and faults working as vertical conduits. Formation and stability of gas hydrate layer in shallow subsurface are most probable connected with the last glacial period Late Weichselian Maximum. Rapid deglaciation could initiate the process of gas hydrate decomposition what, accompanied by continuous supply of free gas from deeper layers, led to enlargement of required storage volume for methane, formation of gas hydrate pingoes, deforming seafloor, and, finally, escape of the large amount of gas, when the structure collapse. Therefore, depressions and mounds are interpreted to be collapse depressions and collapsed hydrate pingoes, respectively, and formed as a result of processes of dynamic formation and decomposition of gas hydrates in shallow subsurface. These structures were formed around 15 ka cal BP, during the retreat of Last Weichselian ice sheet while area was rather unstable.

The subjective nature of the current investigation always leave place for the possibility that some details of the study will be misinterpreted what will lead to the uncertain conclusions; second analysis of the available data or data from the re-survey may lead to the conclusions refinement in the future. Also, prolonged investigations and re-surveys are required to estimate development and observe changes happening with local methane in time perspective.

References

Aber, J. S., Croot, D. G., Fenton, M. M., 1989. *Glaciotectonic Landforms and Structures.* Amsterdam: Springer Netherlands.

Anderson, A. L., Bryant, W. R., 1990. Gassy Sediment Occurence and Properties: Northern Gulf of Mexico. *Geo-Marine Letters 10*, 209-220.

Andreassen, K., Glad, N. E., Ødegaard, C. M., 2007. Analysis of shallow gas and fluid migration within the Plio-Pleistocene sedimentary succession of the SW Barents Sea continental margin using 3D seismic data. *Geo-Marine Letters 27*, 155-171.

Andreassen, K., Laberg, J. S., Vorren, T. O., 2008. Seafloor geomorphology of the SW Barents Sea and its glaci-dynamic implications. *Geomorphology 97*, 157-177.

Andreassen, K., Winsborrow, M., 2009. Signature of ice streaming in Bjørnøyrenna, Polar North Atlantic, through the Pleistocene and implications for ice-stream dynamics. *Annals of Glaciology 50*, 17-26.

Benetti, S., Dunlop, P., Cofaigh, C. O., 2010. Glacial and glacially-related features on the continental margin of northwest Ireland mapped from marine geophysical data. *Journal of Maps*, 14-29.

Benn, D. J., Evans, D. J. A., 1998. *Glacier and glaciation.* London: Arnold.

Berndt, C., Bunz, S., Clayton, T., Mienert J., Saunders M., 2004. Seismic character of bottom simulating reflectors: examples from the mid-Norwegian margin. *Marine and Petroleum Geology 21*, 723-733.

Berndt, C., 2005. Focused fluid flow in passive continetional margins. *Philosophical transaction: Mathematical, Physical and Engineering Science 363*, 2855-2871.

Bluemle, J. P., Clayton, L., 1984. *Large-scale glacial thrusting and related processes in North Dakota.* Boreas.

Bryant, W., Roemer, L., 1983. Structure of the continental shelf and slope of the northern Gulf of Mexico and its geohazards and engineering constraints. In: Geyer R.A. (ed) *Handbook of Geophysical Exploration at Sea.* Bosa Raton, Florida: CRC Press Inc., 123-185.

Capozzi, R., Guido, F. L., Oppo, D., Gabbianelli, G., 2012. *Methane-Derived Authigenic Carbonates (MDAC) in northern-central Adriatic Sea: Relationships between reservoir and methane seepages.*

Cartwright, J., Santamarina, C., 2015. Seismic characteristics of fluid escape pipes in sedimentary basins: Implications for pipe genesis. *Marine and Petroleum Geology 65*, 126-140.

Center for Gas Hydrate, Environment and Climate (CAGE), 2015. *Marine geological cruise to Storfjørdrenna, Bjørnøyrenna and Thor Iversenbanken.*, Tromsø: The Arctic University of Norway.

Elverhøi, A., Antonsen, P., Flood, S.B., Solheim, A., Vullstad , A. A., 1988. The physical environment, western Barents Sea 1:1500000, shallow bedrock geology. *Norsk Polarinstitutt Skrifter 179A*, 32.

Elverhøi, A., Solheim, A., 1987. Shallow geology and geophysics of the Barents Sea. *Norsk Polarinstitutt Rapportserie 37*, 123.

Etiope, G., 2015. *Natural gas seepage.* Amsterdam: Springer.

Gillis, G., 2016. *Slumberger Oilfield Glossary: Goephysics Module.*
Available at: http://www.glossary.oilfield.slb.com/ Accessed 21 May 2016.

Hovland, M., 2012. The Geomorphology and nature of seabed seepage processes. In: Blondel, P. (ed.) *Bathymetry and its applications.* Rijeka: InTech, 79-104.

Hovland, M., Jensen, S., Fichler, C., 2012. Methane and minor oil macro-seep systems — Their complexity and environmental significance. *Marine Geology 332-334*, pp. 163-173.

Hovland, M., Judd, A., Burke Jr., W., 1993. The global flux of methane from shallow submarine sediments. *Chemosphere 26,* 559-578.

Hovland, M., Judd, A. G., 1988. *Seabed pockmarks and seepages. Impact on Geology, Biology and Marine Environment.* London, Dordrecht, Boston: Graham&Trotman (Kluwer).

Hovland, M., Svensen, H., 2006. Submarine pingoes: Indicators of shallow gas hydrates in a pockmark at Nyegga, Norwegian Sea. *Marine Geology 228*, 15-23.

Jamaludin, S. F., Abdul Halim Abdul Latiff, Kadir, A. A., 2015. Interpretation of Gas Seepage on Seismic Data: Example from Malaysiam offshore. *Journal of Physics: Conference Series 664*, 1-6.

Judd, A. G., Hovland, M., 1992. The evidence of shallow gas in marine sediments. *Continental Shelf Research 12,* 1081-1095.

Judd, A., Hovland, M., 2007. *Seabed Fluid Flow. The Impact on Geology, Biology and Marine Environment.* Cambridge: Cambridge University Press.

King, L., McLean, B., 1970. Pockmarks on the Scotian shelf. *Geological Society of American Bulletin 81,* 3141-3148.

Kvenvolden, K. A., Lorenson, T. D., Reeburgh, W. S., 2001. *Attention turns to naturally occuring methane seepage.* Portland: EOS, AGU.

Lammers, S., Suess, E., Hovland, M., 1995. A large methane plume east of Bear island (Barents Sea): implications for the marine methan cycle. *Geol Rundsch 84,* 59-66.

Long, D., Lammers, S., Linke, P., 1998. Possible hydrate mounds within large sea-floor craters in the Barents Sea. *Geological Society. Special Publications 137*, 223-237.
Lucas, M. D., 2015. *The Teacher-Friendly Guide to the Earth Science og the Northwest Central US.* New York: Paleontologic Research Institution.
Løseth, H., Gading, M., Wensass, L., 2009. Hydrocarbon leakage interpreted on seismic data. *Marine and Petroleum Geology 26*, 1304-1319.
Løseth, H., Wensaas, L., Arntsen, B., Hanken, N., Basire, C., Graue, K., 2011. 1000m long gas blow-out pipes. *Marine and Petroleum Geology 28*, 1047-1060.
Melosh, H. J., 1989. *Imact cratering - a geological process.* New York: Oxford University Press.
Paillou, P., El Barkooky, A., Barakat, A., Malezieux, J., Reynard, B., Dejax, J., Heggy, E., 2004. Discovery of the largest impact crater field on Earth inthe Gilf Kebir region, Egypt. *C.R.Geoscience 336*, 1491-1500.
Paull, C. K., Ussler III, W., Dallimore, S. R., Blasco, S. M., Lorenson, T. D., Melling, H; Medioli, B.E., Nixon, F M., McLaughlin, F. A., 2007. Origin of pingo-like features on the Beaufort Sea shelf and their possible relationship to decomposing methane gas hydrates. *Geophysical Research Letters 34*, L01603.
Prior, D., Doyle, E., Kaluza, M., 1989. Evidence of sediment erruption on deep sea floor, Gulf of Mexico. *Science 243*, 517-519.
Serié, C., Huuse, M., Schødt, N., 2012. Gas hydrate pingoes:Deep seafloor evidence of focused fluid flow on continental margins. *Geology 40*, 207-210.
Sheriff, R. E., 2002. *Encyclopedic Dictionray of Applied Geophysics.* Tulsa: Society of Exploration Geophysicists.
Skarke, A., Ruppel, C., Kodis, M., Brothers, D., Lobecker, E., 2014. Widespread methane leakage from the seafloor on the northern US Atlantic margin. *Nature Geoscience 7*, 657-661.
Solheim, A., Elverhøi, A., 1993. Gas-related sea floor craters in the Barents Sea. *Geo-Marine Letters 13*, 235-243.
Sultan, N., Marsset, B., Ker, S., Marsset, T., Voisset, M., Vernant, A.M., Bayon, G., Cauquil, E., Adamy, J., Colliat, J.L., Drapeau, D., 2010. Hydrate dissolution as a potential mechanism for pockmark formation in the Niger delta. *Journal of geophysical research 115*, B08101.
Svendsen, J. I., Gataullin, V., Mangerud, J., Polyak, L., 2003. *The glacial history of the Barents Sea and Kara Sea Region*, Bergen: University of Bergen.

Vorren, T. O., Landvik, J. Y., Andreassen, K., Laberg, J. S., 2011. Glacial History of the Barents Sea Region. In: Ehlers, J., Gibbard, P., Hughes P. (eds.) *Developments in Quaternary Science.* Amsterdam: Elsveier, 361-372.

Winsborrow , M. C., Andreassen, K., Corner, G. D., Laberg, J. S., 2009. Deglaciation of a marine-based ice sheet: Late Weichselian palaeo-ice dynamics and retreat in the southern Barents Sea reconstructed from onshore and offshore glacial geomorphology. *Quaternary Science Reviews 29,* 1-19.